Using Fe-Ti oxides and trace element analysis to determine crystallization sequence of an anorthosite-norite intrusion

Älgön, SW Sweden

Sara Kullberg

Dissertations in Geology at Lund University,
Master's thesis, no 454
(45 hp/ECTS credits)

Department of Geology
Lund University
2015

Using Fe-Ti oxides and trace element analysis to determine crystallization sequence of an anorthosite-norite intrusion

Älgön, SW Sweden

Master's thesis

Sara Kullberg

Department of Geology
Lund University
2015

Table of contents

Cover Picture: Photograph of one single crystal of magnetite. © Alexandra Glommé

Using Fe-Ti oxides and trace element analysis to determine crystallization sequence of an anorthosite-norite intrusion

Älgön, SW Sweden

SARA KULLBERG

Kullberg, S., 2015: Using Fe-Ti oxides and trace element analysis to determine crystallization sequence of an anorthosite-norite intrusion, Älgön SW Sweden. *Dissertations in Geology at Lund University*, No. 454, 32 pp. 45 hp (45 ECTS credits).

The Hakefjorden Complex is an anorthosite-norite intrusion at Älgön, SW Sweden. There are two lithological units associated with it; a marginal monzonorite and a central Ilmenite-Rich Leuconorite (IRL). In the IRL there is a variety of aggregates of Fe-Ti oxides. By investigating Mn-content of ilmenite from all lithological units a chronological order of crystallization could be assessed; oxide aggregates within the IRL → IRL-matrix → anorthosite → anorthosite/norite → monzonorite with monzonorite being the most enriched in Mn and hence the youngest unit. Analysis of incompatible trace elements show that the monzonorite is the most enriched unit and hence also the most evolved and youngest unit of the Hakefjorden Complex. The opposite is true for the oxide aggregates within the IRL. The enrichment in the monzonorite can partly be explained by contamination by the country rock, visible as peaks in Pb, K and Th. Although the contamination is low, r=0.5 (assimilation:fractional crystallization) as deduced by an AFC-model. Furthermore, incompatible trace element ratios show that the magma source is homogenous. As the trace element diagrams lack a U-shape which is indicative of a metasomatically enriched mantle, as well as the double-dip in Nb-Ta, it is not believed that the magma originates from an enriched mantle. Finally, as the Th concentration is low, as opposed to levels in the upper crust, it is theorized that the Hakefjorden Complex originates from a lower mafic crust.

Keywords: anorthosite-norite, ilmenite-rich leuconorite, ilmenite, AFC-model, magma origin

Supervisor: Anders Scherstén

Subject: Bedrock Geology

Sara Kullberg, Department of Geology, Lund University, Sölvegatan 12, SE-223 62 Lund, Sweden. E-mail: sara.kullberg@hotmail.com

Analys av Fe-Ti oxider samt spårämnesanalys för att bestämma kristallisationsordningen i ett anortosit-norit-komplex

Älgön, SV Sverige

SARA KULLBERG

Kullberg, S., 2015: Analys av Fe-Ti oxider samt spårämnesanalys för att bestämma kristallisationsordningen i ett anortosit-norit-komplex. *Examensarbeten i geologi vid Lunds universitet*, Nr. 454, 32 sid. 45 hp.

På Älgön, SV Sverige, finns en anortosit-norit intrusion tillhörande Hakefjordenkomplexet. Det finns dessutom två tillhörande enheter; en marginell monzonorit och en centralt belägen ilmenitberikad norit (IRL). I den ilmenitberikade noriten finns även olika sorters aggregat av Fe-Ti oxider. Genom att undersöka Mn-innehållet i ilmenit i alla litologiska enheter var det möjligt att få fram en kronologisk kristallisationsordning; oxidaggregat i IRL → IRL → anortosit → anortosit/norit → monzonorit, där monzonoriten är mest rik på Mn och därmed yngst. En analys av inkompatibla spårämnen visar även på att monzonoriten är den mest berikade enheten och därmed den mest utvecklade och yngsta enheten i Hakefjordenkomplexet. Tvärtom är det för oxidaggregaten i den ilmentiberikade noriten. Dock beror berikningen i monzonoriten även delvis på kontamination av omkringliggande bergart; toppar av Pb, K och Th indikerar detta. En geokemisk modellering (AFC) visar på att förhållandet mellan kontaminering och kristallisation är 0.05, det vill säga låg. Fortsättningsvis visar förhållanden mellan inkompatibla spårelement att källan för magman är homogen. Eftersom spårelementkurvan i ett spindeldiagram ej innehar en U-form, vilket är indikativt för en mantelkälla som har blivit berikad av metasomatiska fluider, eller har negativa anomalier för både Nb och Ta är det inte troligt att magman har sitt ursprung i manteln. Slutligen, eftersom Th koncentrationen är låg är det inte troligt att källan är en övre skorpa utan snarare en undre, mafisk skorpa.

Nyckelord: anortosit-norit, ilmenitrik norit, ilmenit, AFC-modell, magmakälla

Handledare: Anders Scherstén

Ämne: Berggrundsgeologi

Sara Kullberg, Geologiska institutionen, Lunds Universitet, Sölvegatan 12, 223 62 Lund, Sverige. E-post: sara.kullberg@hotmail.com

1 Introduction

Älgön on the south-western coast of Sweden is a spectacular island, both in a scenic and in a geologic way, being part of the Hakefjorden Complex (HFC). At Älgön and its neighboring island Brattön several rock units occur together, such as the paragneiss Stora Le-Marstrand (SLM), pegmatites, ultramafic lenses, an anorthosite-norite intrusion and granitic- as well as doleritic dykes. The anorthosite-norite intrusion, which occurs on both islands, is *sensu strictu* the Hakefjorden Complex. Additionally, in the central parts of Älgön there is an enrichment of Fe-Ti oxides (Årebäck 1995). Fe-Ti oxide aggregates are often associated with Proterozoic massif anorthosites and commonly inhibit a subeconomic to economic value (Ashwal 1993). The extent of the Fe-Ti enriched area on Älgön is too small for being economically profitable and mining is therefore not carried out. Moreover, the island has a very rich flora and fauna and is therefore classified as a nature reserve and hence protected by Swedish law (Fahlén *et al.* 2008; Länsstyrelsen 2015).

The Fe-Ti oxide aggregate, called Ilmenite-Rich-Leuconorite (IRL, Årebäck 2001), inhibits several smaller subunits, described in more detail below. How and why there is an IRL, as well as how the norite, anorthosite and IRL are connected is still debatable. Anorthosites, in general, are enigmatic as to how they are formed and what their origin is (e.g. Ashwal 1993; Duchesne *et al*. 1999; Schiellerup *et al*. 2000). There have been several attempts to solve the puzzle of the Hakefjorden Complex (e.g. Årebäck 1995; 2001), although none completely successful. Here I build on previous work and aim at answering the following:

- Is it possible to elucidate the relationship between the units in the complex simply by investigating the Fe-Ti oxides?
- Is an AFC-model (Assimilation:Fractional crystallization) developed by DePaolo (1981), feasible?
- Is it possible to deduce whether the magma originates from the mantle or the continental crust by looking at trace element signatures?

The goal is to get a better understanding of the overall mechanisms behind the formation of the Hakefjorden Complex.

2 Fe-Ti oxides

Ilmenite ($FeTiO_3$) and to some extent magnetite (Fe_3O_4) are important minerals within the Hakefjorden Complex. They are both susceptible to changes in oxygen conditions as they contain iron. As the amount of oxygen in a system governs which minerals that crystallize and in what order due to its effect on the Fe^{3+}/Fe^{2+} ratio, it is important to understand the concept of oxygen fugacity. Therefore, a short review of the concept will follow.

2.1 The role of oxygen fugacity

Oxygen fugacity (fO_2) can be explained as to how much oxygen there is in a magmatic system (Brownlow 1996). O_2 is almost never found as a pure phase in geologic environments, but is bound to other phases, such as in H_2O or CO_2. To get an indication of how oxidized the environment is one can study the Fe^{3+}/Fe^{2+} ratio. An oxidized magma has a higher Fe^{3+}/Fe^{2+} ratio compared to a more reduced magma. As the Fe-Ti oxides have different Fe^{3+}/Fe^{2+} ratios, the Fe^{3+}/Fe^{2+} in the magma will control which oxide that will crystallize. A high Fe^{3+}/Fe^{2+} ratio will lead to saturation of magnetite before ilmenite, and a lower ratio will lead to saturation of ilmenite before magnetite (Frost 1991).

There are several factors that govern the oxygen fugacity, such as amount of fluids and their chemistry, crystallization sequence and the chemistry of the magma itself. For example, if Mg is present in a system, ferrous iron will be stabilized at a higher oxygen fugacity, thus indicating a low Fe^{3+}/Fe^{2+} even though the magma is oxidized. To conclude, it is important to understand that it is impossible to look at only the Fe^{3+}/Fe^{2+} when assessing the oxidation state of the magma (Frost 1991).

Nevertheless, there are certain mineral reactions that are said to buffer the fO_2, so called redox-buffers (Fig. 1). As long as all phases in a buffer is present the oxygen fugacity will not deviate much from values represented by the buffer. Two of the most common are the Fayalite-Magnetite-Quartz (FMQ) and the Magnetite-Hematite (MH, Frost 1991);

$2Fe_3O_4+3SiO_2 \leftrightarrow 3Fe_2SiO_4+O_2$ (FMQ)

$6Fe_2O_3 \leftrightarrow 4Fe_3O_4+O_2$ (MH)

In all reactions, the products to the left are the more oxidized whereas the right part is more reduced.

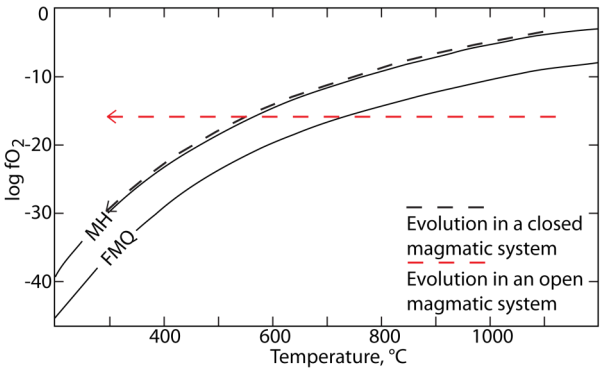

Fig. 1. This figure depicts the relationship between oxygen fugacity and temperature in a magmatic system. The buffers in this figure are MH and FMQ which are described in the text. The oxygen fugacity can evolve either along a buffer or crossing one, depending on if the system is closed or open. As depicted in the figure, an open system can become relatively more oxidized due to addition of fluids. Typical for a magmatic system is that the oxygen fugacity does not deviate much from fugacities implied by a buffer (like the one following the MH). In common for the two buffers depicted is that they are more oxidized above the buffers, compared to below. Modified after Buddington and Lindsley (1964).

2.2 Exsolution and oxidation

Magnetite is part of the magnetite-ulvöspinel (Fe_3O_4–Fe_2TiO_3) solid solution series and ilmenite is part of the ilmenite-hematite ($FeTiO_3$–Fe_2O_3) solid solution series. Abbreviations will be as follows: Mt–Usp_{ss} and Ilm–Hem_{ss}, after Buddington and Lindsley (1964). The complete list of abbreviations can be found in appendix I. At high temperatures the solid solutions are complete, but at around 600°C a miscibility gap occurs for both series (Lindsley 1991), and exsolution-reactions take place. Alongside with exsolution, oxidation often occurs simultaneously.

In ilmenite lamellae of hematite is a result of subsolidus exsolution and not oxidation. Oxidation follows the steps R1–R7 as defined by Haggerty (1991):
R1: homogenous ilmenite without exsolutions
R2: ferrian ilmenite + ferrian rutile
R3: ferrian rutile + ferrian ilmenite
R4: rutile + titanohematite + ferrian rutile + ilmenite
R5: rutile + titanohematite
Steps R6–7 are uncommon and require extremely high fO_2. The oxidation results in a more complicated intergrowth of rutile and titanohematite and the addition of pseudobrookite (Haggerty 1991).

Another oxidation reaction where ilmenite is altered to titanite was proposed by Harlov *et al.* (2006). This is also done in the presence of a fluid, although of a different character:
$cpx+ilm+qz+H_2O \leftrightarrow amph+tit$
$amph+ilm+O_2 \leftrightarrow tit+mt+qz+H_2O$

Oxidation of magnetite is somewhat more complex and often occurs close after exsolution of ulvöspinel. It is thought to follow the steps below according to Haggerty (1991):
C1: the magnetite is homogenous with Usp in complete solid solution.
C2: $6Fe_2TiO_4 + O_2 \leftrightarrow 6FeTiO_3 + 2Fe_3O_4$. The Usp-component in Mt-Usp_{ss} oxidizes to ilmenite and a more magnetite-rich Mt-Usp_{ss}. As a consequence small lamella of ilmenite form within the magnetite.
C3: $4Fe_2TiO_4 + O_2 \leftrightarrow 4FeTiO_3 + 2Fe_2O_3$. The Usp-component is further oxidized and the ilmenite lamellas grow and hematite forms.
C4–C6: further oxidation results in a transition to rutile and titanohematite, similar to step R5 for ilmenite.

As the previous reactions have shown, increasing the fO_2 will lead to a greater Hem-component in ilmenite and a smaller Usp-component in magnetite (Buddington & Lindsley 1964).

The compositions of the series are further governed by temperature; with increasing T the more ulvöspinel and hematite there is in the Mt-Usp_{ss} and Ilm-Hem_{ss} (Fig. 2, Buddington & Lindsley 1964; Charlier *et al.* 2015). The equilibrium reaction governing the solid solution series' composition is:
$Fe_2TiO_4+Fe_2O_3 \leftrightarrow Fe_3O_4+FeTiO_3$
Where the exchange is $Fe^{2+}+Ti^{4+} \leftrightarrow 2Fe^{3+}$.
This reaction is extremely temperature dependent and is therefore a tool for calculating the temperature and oxygen fugacity during crystallization of the formation. Furthermore, the reaction is pressure-independent (Lindsley 1991). Although oxides suffer subsolidus re-equilibriation such as oxidation and exsolution (Haggerty 1991; Lindsley 1991), the Fe/Ti ratio is thought to remain constant. Assuming no mass-transport has occurred, it would be possible to estimate the temperature of formation (Lindsley 1991 and references therein).

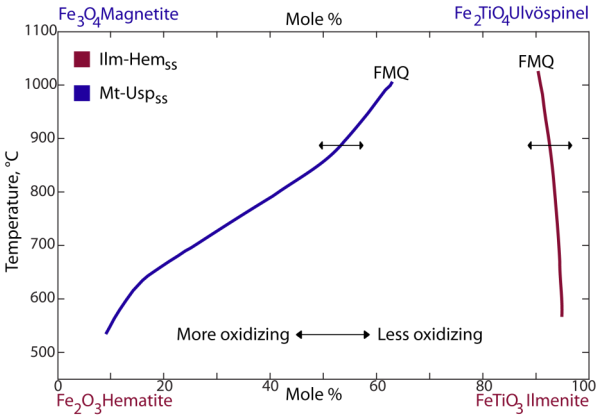

Fig. 2. This figure depicts how the composition of the solid solution series change with temperature. The two curves depict either Mt-Usp_{ss} (blue) or Ilm-Hem_{ss} (red). As it is visible in the figure, Mt-Usp_{ss} is more susceptible to changes in temperature. For example, magnetite that crystallizes at 1000°C will have 60 wt% Usp, whereas it will have 25-30 wt% Usp when crystallizing at 700°C. The same scenario for ilmenite gives 10 wt% Hem at 1000°C and 5 wt% at 700°C. Modified after Buddington and Lindsley (1964).

3 Magma differentiation

A magma that undergoes crystallization can be affected by numerous differentiation-processes, such as fractional crystallization or assimilation of country rock material, or a combination of both (Winter 2009).

3.1 Assimilation and fractional crystallization

Assimilation is the process when a magma is contaminated by alien material. Since melting a material requires substantial energy, which is provided by latent heat from crystallization, assimilation is usually rather low. It has been estimated that to melt 1 g of rock, 3 g of melt must crystallize (Winter 2009).

Adding material to a melt has different effects on major element concentrations compared to trace element concentrations. Major elements are insensitive whereas trace elements concentrations vary depending on partition coefficients and amount of melt generated. As trace elements are incompatible they enter the melt over the crystalline phase. The smaller the amount of melt and the lower the partition coefficient, the higher the concentration of trace element in the melt generated (Fig. 3, Winter 2009).

When material, in the form of formed crystals, is removed it is called fractional crystallization. Depending on e.g. density contrasts crystals can either float or

sink, forming cumulates. The chemistry of the remaining magma depends on which phase that crystallizes. An element compatible in the crystallizing phase will be depleted in the remaining magma and vice versa if the element is incompatible (Winter 2009).

3.2 Combined assimilation and fractional crystallization

The combined effects of assimilation and fractional crystallization have been modeled by DePaolo (1981) in the so called AFC-modeling (Assimilation:Fractional Crystallization). How magma chemistry changes with varying degrees of assimilation and fractional crystallization is summarized in figure 4. The basic equation for describing the combined effects is:

$$\frac{d\mu}{dt} = M_a C_a - M_c D C_m$$

The equation describes the concentration of a certain element (μ) at a given time. M_a is the rate at which wall rock assimilates and C_a is the concentration of the certain element in the assimilated material. M_aC_a therefore describes the addition of the chosen element to the system. M_cDC_m on the other hand describes the removal of the element from the magma by fractional crystallization. Here, M_c describes the rate of crystallization, D is the partition coefficient and C_m is the concentration of the element in the magma. If the contaminant is a result of partial melting of the wall rock the concentration of the added element (C_a) will be C_w/D', where C_w is the concentration of the element in the wall-rock and D' is the distribution coefficient between solid/liquid. An important factor when modeling is the r-value which depicts the ratio assimilation:fractional crystallization.

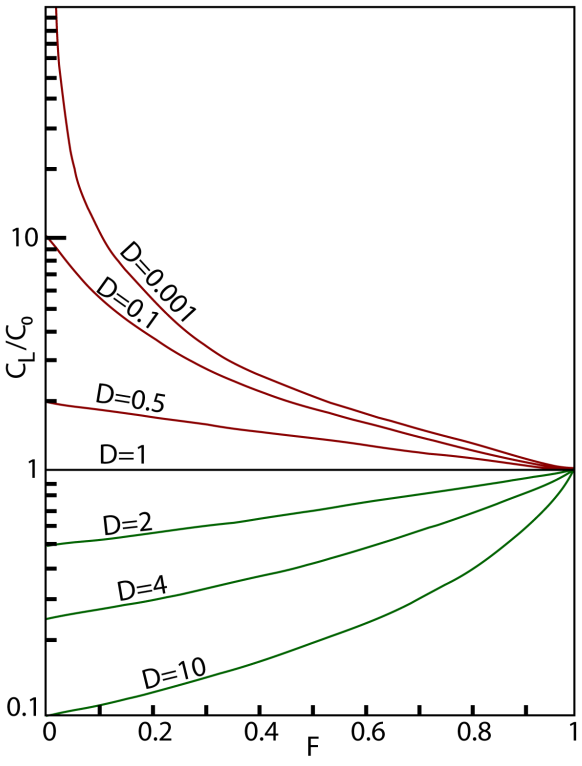

Fig. 3. The figure shows how the concentration of an element in a melt varies between compatible and incompatible elements. Compatible elements have D-values ≥1 whereas incompatible elements have D<1. C_L/C_0 is the concentration ratio of an element between the melt generated and the original material. Incompatible elements enter the liquid easily, depicted as high C_L/C_0 for low values of F (melt generated), whereas compatible elements remain in the solid phase. Modified after Winter (2009).

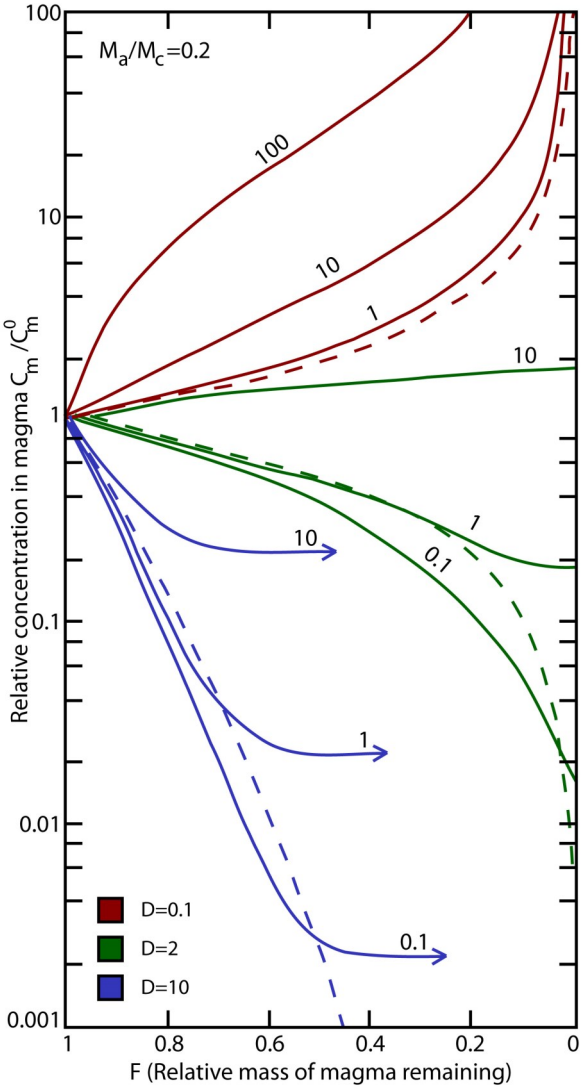

Fig. 4. Three main scenarios are illustrated in the figure: incompatible elements (red), compatible elements (green) and extremely compatible elements (blue). The dashed lines represent magma differentiation by fractional crystallization only. M_a/M_c is the ratio of assimilation to fractional crystallization (r-value) and in this figure set to 0.2. The numbers on the curves is the ratio C_a/C_m^0 where C_a is the concentration of an element in the assimilated material and C_m^0 is the concentration in the original magma. In general for all three scenarios is that by increasing the concentration of an element in the assimilated material (numbers 1-10-100 on curves) leads to a drastic increase in concentration in the remaining magma even though fractional crystallization occurs simultaneously. Modified after DePaolo (1981).

4 Geologic setting

The area of interest crops out on the islands of Älgön and Brattön (Fig. 5a). The rocks are better exposed on Älgön, which is also the focus of the study.

4.1 Pre-sveconorwegian

The Fennoscandian shield can be divided into several units (Fig. 5b). The oldest unit is to the east and was formed during the Svecokarelian orogeny. During this event, 1.91-1.86 Ga, several micro-continents were amalgamated and accretionary growth created the core of Fennoscandia (Åhäll & Connelly 2008).

Following the orogeny, subduction related magmatism, including the Transscandinavian Igneous Belt (TIB; 1.8-1.65 Ga), took place at the western margin of the evolving Fennoscandian protocrust for approximately 330 Ma. (Gorbatschev & Bogdanova 1993; Åhäll & Larson 2000).

West of the Fennoscandia foreland there are two units, the Eastern segment and the Idefjorden terrane. The former consists of granitoid gneisses whereas the latter consists of metamorphosed sediments as well as intrusive rocks (Åhäll & Connelly 1998). These terranes were affected by metamorphism and reworking during the Sveconorwegian orogeny (1.15-0.9 Ga) (Söderlund *et al*. 2002).

The Idefjorden terrane consists of several identifiable units (Fig. 5a), which are the Horred formation, Göteborg-Åmål belt, the Stora Le-Marstrand (SLM) formation and the Hisingen suite, where Horred is the oldest and the Hisingen suite, the youngest. They are all thought to have formed in an outboard island arc or back arc tectonic setting, during the supposed Gothian orogeny (Åhäll & Connelly 2008). The SLM contains metasediments, predominantly metagreywackes and amphibolites of supracrustal ± intrusive origin which were possibly deposited at 1.59 Ga (Åhäll *et al*. 1998).

The SLM can further be divided into SLM1 (1.59 Ga) and SLM2 (1.57–1.55 Ga), where the division is marked by intrusion of the Hisingen suite rocks, which are also subduction related (Åhäll *et al*. 1998; Åhäll & Connelly 2008).

4.2 Sveconorwegian orogeny

The previous described units were more or less affected by the Sveconorwegian orogeny. The evolution of the orogeny has been reviewed by Bingen *et al.* (2008). The most common belief is that the orogen is a result from a collision between Laurentia-Baltica and the continent of Amazonia that took place between 1140 and 900 Ma (Bingen *et al.* 2008). However, it has recently been suggested by Slagstad *et al.* (2013) that the Sveconorwegian orogeny in Baltica is an accretionary orogeny that does not involve Himalayan style continental collision. This hypothesis is debatable (Möller *et al.* 2013; Slagstadt *et al*. 2013), and I here assume the more classic interpretation of a continent-continent collision. The orogeny can further be divided into four phases (Bingen *et al.* 2008);

1: Arendal phase (1140–1080 Ma): represents collision between Idefjorden terrane and Telemarkia terrane through closure of an ocean.
2: Agder phase (1050–980 Ma): main Sveconorwegian phase with continent-continent collision.
3: Falkenberg phase (980–970 Ma): represents the last phase of the collision before divergence.
4: Dalane phase (970–900 Ma): the orogen collapsed and post-collisional intrusions took place.

Of the above phases, the Dalane phase is the most important for this work as the Hakefjorden Complex formed towards the end of this period. Below follows a short review of post-collisional intrusions along the Swedish west coast, and are listed in chronological order from oldest to youngest. The Hakefjorden Complex is the youngest intrusion of the Dalane phase and is further described in section 5.

4.2.1 Vinga intrusion

One of the first intrusions during the Dalane phase was the Vinga intrusion, named after the island of Vinga. It outcrops south of the Hakefjorden Complex (Fig. 5a). It displays igneous textures and is undeformed. The composition ranges from a plagioclase porphyritic granite to a quartz jotunite, and the SLM metagreywackes. The intrusion has been dated to 951±7 Ma by U-Pb dating in zircon (Årebäck *et al.* 2008). Additionally, the intrusion has several features in common with the Hakefjorden Complex such as mafic enclaves and the associated hybrid rock (Årebäck *et al.* 2008).

4.2.2 Göteborg dykes

In the Göteborg area a swarm of WNW-W trending mafic dykes can be found. They are all thought to represent post-kinematic conditions of the Sveconorwegian orogeny and thus to be a part of the Dalane phase. They have a monzonoritic composition and infrequent plagioclase megacrysts can be found. These two features can also be found on Älgön, which will be discussed more in detail further below. Contamination cannot be ruled out since xenoliths of wall rock have been found within the dykes. The dykes display igneous textures and chilled margins and they are undeformed. They crosscut the country rock obliquely to the metamorphic fabric. U-Pb in zircon yield an age of 935±3 Ma (Hellström *et al.* 2004).

4.2.3 Bohus granite

The Bohus Granite crops out over an area of 2000 km^2 just north of Hakefjorden Complex, see figure 5a. It consists of a suite of granitic intrusions with variable petrography and chemistry (Eliasson *et al.* 2003). As a whole, the Bohus granite overlaps the Hakefjorden Complex in age. U-Pb analysis of monazite and xenotime yields ages of 919±5 and 922±5, respectively. It displays magmatic textures and is believed to be post-kinematic (Eliasson & Schöberg 1991).

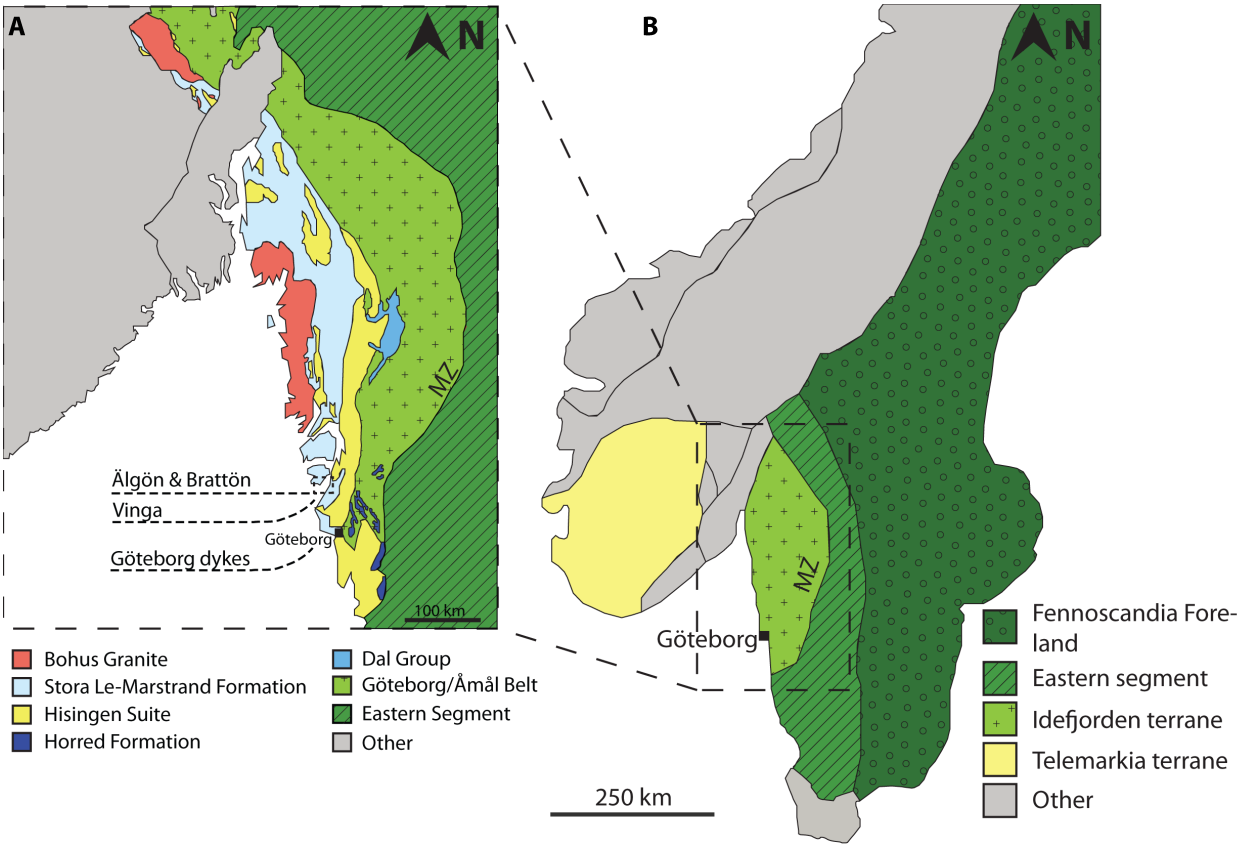

Fig. 5. a) The Idefjorden terrane contains the Horred formation, Göteborg-Åmål belt, the Stora Le-Marstrand (SLM) formation and the Hisingen suite. The Hakefjorden Complex (Älgön & Brattön) is marked in the figure, as well as the other late Sveconorwegian intrusions. MZ = Mylonite Zone. A better figure of Älgön is provided later in figure 6. (Modified after Petersson *et al*. 2015). *b)* The Fennoscandian shield is divided into several units; Fennoscandia Foreland, the Eastern Segment and the Idefjorden terrane. The Telemarkia terrane in western Norway is included as it contains several similar anorthosite-norite intrusions as the Hakefjorden Complex. Modified after Åhäll and Connelly (2008).

4.2.4 Rogaland intrusive massifs

Further westward, in SW Norway the Rogaland anorthosite province (Telemarkia terrane, Fig. 5b) is located and bears many similarities to the Hakefjorden Complex. The province is further divided into three anorthositic massif bodies; Egersund, Håland-Helleren and Åna-Sira (Duchesne & Bingen 2001). In the latter province, one of the world's largest deposits of Fe-Ti oxides can be found; namely the Tellnes ilmenite deposit (Charlier *et al*. 2006). Just as the Hakefjorden Complex, the Rogaland anorthosite massifs post-date the Sveconorwegian deformation (Schärer *et al*. 1996; Duchesne *et al*. 1999). Nevertheless, the massifs have undergone some deformation but this is believed to be due to diapiric emplacement of the complex (Schärer *et al*. 1996). Zircon U-Pb dating yielded an emplacement age of approximately 930 Ma. Interestingly, the Fe-Ti oxide deposit was dated to 920±3 Ma, thus post-dating the anorthosite bodies (Schärer *et al*. 1996).

Similar to the Hakefjorden Complex the final emplacement of the complex was at about 5 kbar (Vander Auwera & Longhi 1994).

5 Hakefjorden Complex

The Hakefjorden Complex is an anorthosite-norite intrusion (Årebäck 1995). The P/T-conditions of the emplacement has been estimated to 3.7–6.4 kbar and 890–1015°C (Årebäck & Andersson 2002). P/T estimates were obtained from mineral equilibria along the contact areole of the peraluminous country rock (SLM). The Hakefjorden Complex consists of four main units; norite, monzonorite, anorthosite and an Ilmenite-Rich Leuconorite (IRL, Fig. 6). The units are thought to have formed through a combination of fractional crystallization and country rock assimilation, presumably metasedimentary rocks of the Stora Le-Marstrand Formation (SLM) (Årebäck 1995; Årebäck & Stigh 2000; Årebäck 2001). The age of the emplacement was determined through U-Pb in a zircon derived from an anatectic melt in the country rock. It is believed that the melt is a direct result from the intrusion of the complex and was dated to 916±11 Ma (Scherstén *et al.* 2010). As the island has undergone brittle deformation steep cliffs and valleys is a prominent feature (Årebäck 1995). The island is therefore best seen from afar (Fig. 7a). Additionally, the island is covered in vegetation (Fig. 7b).

Blocks of monzonorite occasionally occur within the norite, just as blocks of norite occasionally occur within the IRL (Årebäck 1995; Årebäck & Stigh 2000; Årebäck 2001). The IRL-unit is further divided into several subunits (Årebäck & Stigh 2000; this thesis

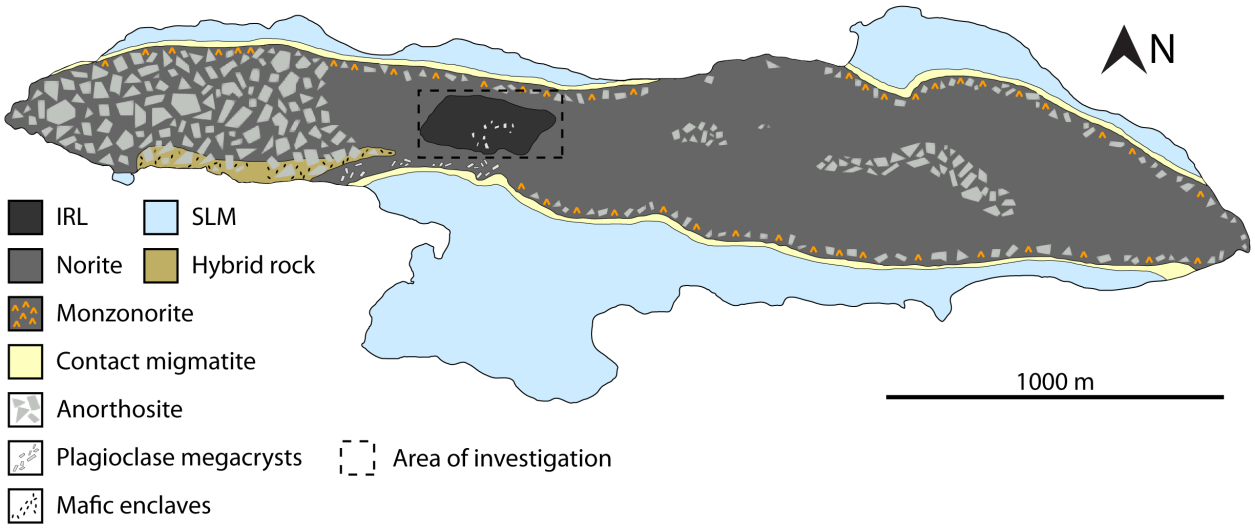

Fig. 6. The figure depicts how the different lithological units on Älgön are distributed. The Stora Le-Marstrand (SLM) formation (light blue) is not part of the Hakefjorden Complex but is the host rock. As it is visible, the monzonorite occurs as an outer rim to the norite-anorthosite complex, directly in contact with the host rock. The area of investigation is marked in the figure. Several pegmatite veins and dykes of various compositions are not included in the figure as they are not covered by the scope of this thesis. Modified after Årebäck (1995).

section 7.1). Furthermore Årebäck & Stigh (2000) observed that the IRL exhibits magmatic foliation, which has not yet been reported elsewhere on the island. They also suggested that the IRL-unit formed during ascent of a continuously fractionating magma, resulting in pockets of oxide-enriched material. The oxides in these pockets settled and created a primary foliation. Theses pockets were later disturbed and deformed and the foliation was disrupted and the different subunits were formed.

The anorthosite is thought to have formed through crystallization in a polybaric environment. The anorthosite is assumed to have started to crystallize in a deep-seated magma chamber, of unknown affinity, where it formed a floatation cumulate. Thereafter, the magma started to rise and was finally emplaced at 3.7–6.4 kbar and 890–1015°C (Fig. 8, Årebäck & Stigh 1997; Årebäck & Andersson 2002). This polybaric evolution resulted in megacrysts with partly resorbed rims. At P/T-conditions during the final emplacement, the megacrysts continued to grow, covering the resorbed rim with normally zoned plagioclase (Årebäck & Stigh 1997). An alternative hypothesis in order to explain the complex zoning pattern in the plagioclase megacrysts is the injection of a more primitive magma that lead to increasing An-content in the later plagioclase (Scherstén pers. com. 2015). However, the work from Glommé (2015) seems to suggest homogenous Sr -isotope composition in the plagioclase of the Hakefjorden Complex, which does not readily support the latter hypothesis.

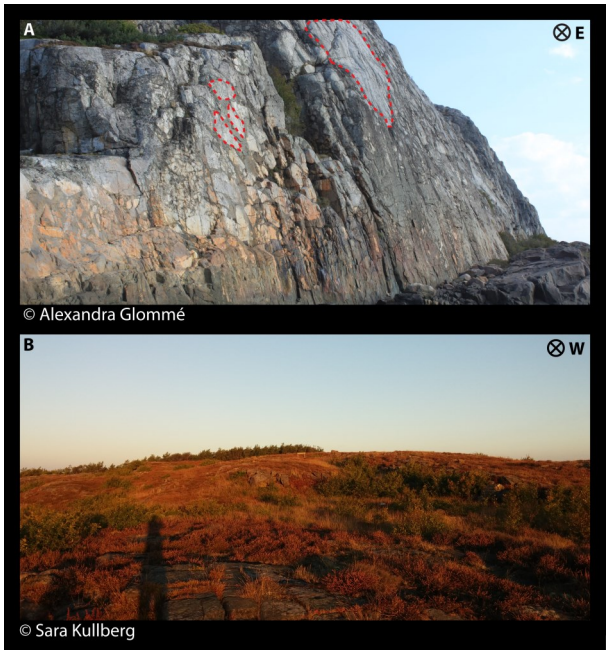

Fig. 7. a) One wall showing how the anorthosite floats around in the norite and how it tends to float upwards. Some blocks are marked by red dashed lines. As it is visible in the photograph, the blocks of anorthosite are very different in size. *b)* Almost the entire field area is visible in this photo. It extends over a few 100m^2 and is essentially covered completely in lichen and heather. Luckily there are sheep on the island grazing and keeping the vegetation low.

6 Methods

The methods used for reaching the goal of the thesis can be divided into three parts; one practical part with field work, one practical part with laboratory work and one theoretical part with geochemical modeling combined with literature studies.

6.1 Fieldwork

The aim of the fieldwork was to study the IRL with the associated subunits, due to its enrichment in oxides. Apart from mineralogy and textures, some focus was also on the internal relationships between the subunits.

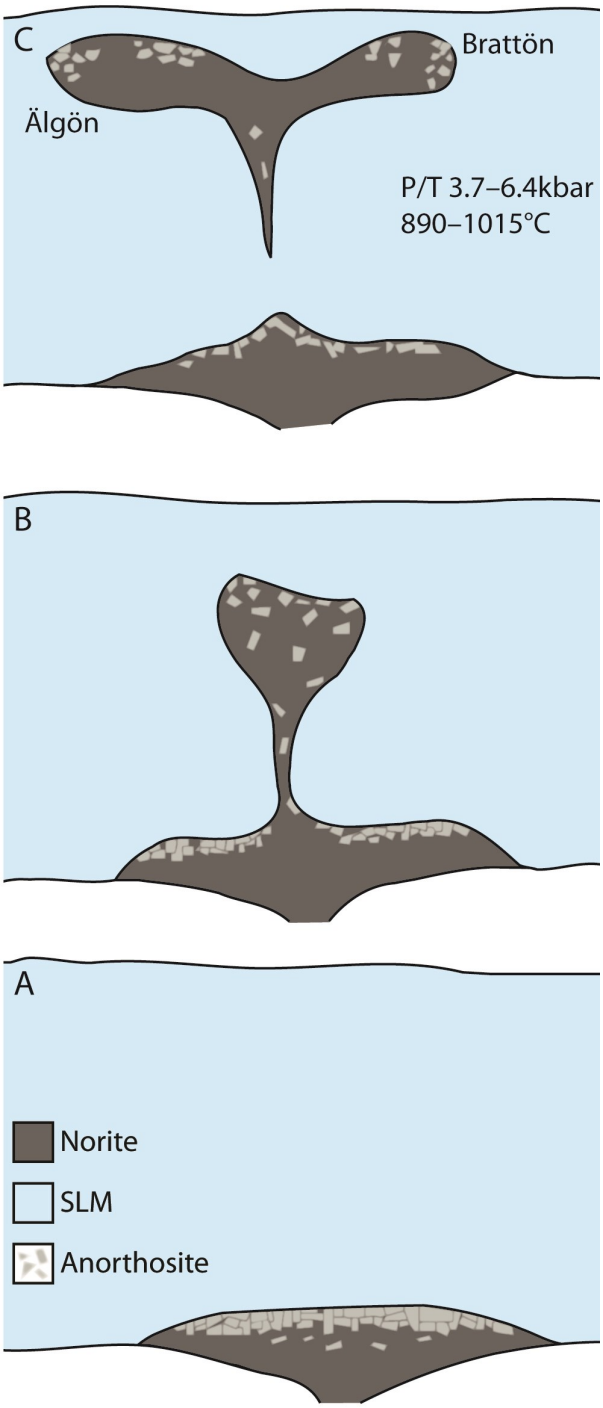

Fig. 8. A model showing how Årebäck and Stigh (1997) theorized the evolution of the Hakefjorden Complex based on the textural appearance of plagioclase megacrysts. The P/T-conditions in the deep-seated magma chamber remains unknown. *a)* Plagioclase accumulates at the roof of the magma chamber. *b)* The magma starts to rise and the plagioclase megacrysts are in dis-equilibrium. Here it is theorized by Årebäck and Stigh (2000) that the IRL started to crystallize. *c)* The plagioclase megacrysts are once again in equilibrium. Anorthosite floats upwards and accumulate at what will become the outer rims of Älgön and Brattön. Modified after Årebäck and Stigh (1997).

The area of investigation can be seen in figure 6 and 7b. As seen in the figures, the area is small, expanding over an area of a few hundreds of square meters. After visual examination, samples were collected for further analysis. Samples were collected from other localities as well, in order to get representative samples of all lithological units represented in this thesis. Exact coordinates for the samples can be found in appendix II.

6.2 Laboratory work

Samples were crushed by hand and pulverized with a C-W mill to minimize the risk of contamination. The powders were sent to ACME lab, Canada, for bulk rock analysis. Analysis package LF202 was chosen due to its extensive list of elements analyzed. For complete list of elements analyzed and the detection limits, the reader is referred to ACME's 2014 Schedule of Services and Fees (Appendix III). The results were thereafter modeled using the computer software IgPet.

Samples were also sent to the Geological Institute, Slovak Academy of Sciences (SAS), for production of thin-sections. Some samples were also molded into an epoxy mount and thereafter polished at the Dept. of Geology, Lund University. Both mounts and thin-sections were examined under an optical microscope as well as in a Hitachi 3400N SEM (Scanning Electron Microscope) with an Oxford EDS system and a Gatan Mini-CL system. Special focus was on Fe-Ti oxides and their main element chemistry as well as their textural appearances.

7 Results

The fieldwork and following lab work resulted in a refinement of what sorts of inclusions could be found within the IRL-unit. One inclusion, a small one with laminations of oxides and plagioclase, is not described herein because of difficulties getting a sample. For further description, see "laminated inclusion" in Årebäck and Stigh (2000).

7.1 IRL and its inclusions

7.1.1 Oxide aggregate

The oxide aggregate consists of ilmenite with a bimodal grain size, 1–3mm. They are anhedral and rounded. Ilmenite form triple junctions and with sharp and unaltered contacts. Ilmenite is optically homogenous but sometimes show hematite exsolutions, which are visible in SEM, see figure 9a. Some ilmenite grains have kink-bands made visible by hematite lamellae (Fig. 9b). Overall mineralogy is 95% ilmenite with interstitial plagioclase and titanaugite, which are poikilitic and form heteradcumulates.

7.1.1.1 Oxide aggregate with snowflake-textured plagioclase

The appearance is almost identical to that of the previous oxide aggregate. The ilmenite grains have a bi-

modal grain size, 0.5–3mm. They are also anhedral and rounded as opposed to magnetite that is anhedral and more angular. Ilmenite form triple junctions and with sharp and unaltered contacts. Ilmenite is optically homogenous although hematite lamellae are visible in the SEM. When ilmenite is in contact with magnetite, hematite lamellae also become visible under the optical microscope. The contacts between magnetite-ilmenite are altered. Magnetite has Trellis lamellae of ilmenite (Fig. 9c).

The snowflake-like textures, also called "snowflakes", are poikilitic plagioclase, 3–5mm. Small grains of ilmenite occur as inclusions within these. Interstitial minerals are poikilitic plagioclase and titanaugite, forming heteradcumulates (Fig. 9d).

7.1.2 Magnetic veins

Ilmenite and magnetite display a grain size range, 1–3mm. The modal ratio between them is 9:1 (ilmenite:magnetite). The ilmenite grains are anhedral, and rounded whereas the magnetite is anhedral but angular. Ilmenite meet in triple junctions and contacts ilmenite-ilmenite are sharp and unaltered as opposed to contacts to magnetite which are reacted. Ilmenite is either homogenous or has hematite lamellae. These lamellae decrease in abundance toward bordering magnetite grains, but increase toward cracks. Magnetite has Trellis lamellae of ilmenite. Randomly distributed baddeleyite inclusions occur in ilmenite, (Fig. 9e). Interstitial titanaugite creates heteradcumulates.

7.1.3 Sugary anorthosite

The grains of plagioclase in this type of inclusion are lath-shaped and display a homogenous grain size of 0.5mm. The ilmenite grains are rounded and occur as inclusions in the plagioclase. They range from 0.1–0.5mm in size.

7.1.4 Grey inclusion

The grey inclusion consists of an outer rim and a central part. The outer rim consists solely of lath-shaped plagioclase with homogenous grain-size, 0.5mm, whereas the central part display more phases. The central phase is mottled with undistinguishable phases as well as rounded oxide. One phase is brownish in plane polarized light (ppl), shows no pleochroism and has high interference colors in crossed polarizers (xpl). No sufficiently qualitative measurements of either phase in the central part were achieved in the SEM.

7.1.5 IRL-matrix

The ilmenite in the IRL-matrix shows a homogenous grain size, 1mm. The grains are subhedral to anhedral and display sharp and unaltered contacts to other phases. When grains of ilmenite occur close together they are more anhedral and rounded and display triple junctions. Ilmenite is an interstitial phase to ophitic plagioclase. The latter is oriented making the matrix anisotropic (Fig. 9f).

The ilmenite is homogenous but sometimes lamellae of hematite occur, barely visible in optical microscope. Ilmenite with further exsolutions is uncommon. Randomly oriented baddeleyite occur as inclusions in ilmenite.

7.2 Lithological units

7.2.1 Norite

Two norite samples were investigated, one altered and one unaltered. The altered sample was collected during field work for this thesis whereas the unaltered sample was collected during previous field work. The altered norite was found as an inclusion within the IRL. In the unaltered sample, the main mineralogy was plag+opx+cpx+ilm with secondary minerals of hbln+chl. Oxides are anhedral, 0.5–5mm. Ilmenite is homogenous and skeletal (Fig. 10a), following the terminology of Årebäck (1995), or with weak exsolutions of hematite. Ilmenite and magnetite no longer occur as aggregates but more as individual grains found evenly distributed throughout the sample. When ilmenite is occurring together with magnetite, there is no reaction rim between the two phases. The magnetite has Trellis lamellae of ilmenite.

In the altered sample, oxides also occur as exsolved phases from primary pyroxenes, see Fig. 10b. The pyroxenes have been altered to hornblende and chlorite. Ilmenite has exsolutions of both rutile and hematite. Magnetite has weak Trellis lamellae.

7.2.2 Monzonorite

The main mineralogy is plag+amph+chl+opx+cpx ilm+qz. All phases have approximately the same grain size of 2mm. Oxides can be found as exsolved phases within primary pyroxene, which are further altered to amphiboles. Both ilmenite and magnetite are small, 0.1 mm, and anhedral-subhedral. Ilmenite is skeletal/anhedral with rims of titanite (Fig. 10c). Magnetite has Trellis lamellae/sandwich lamellae of ilmenite. These lamellae are sometimes altered to titanite. Abundant elongate grains of zircon were found throughout the sample (Fig. 10d).

7.2.3 Anorthosite

Rounded ilmenite, size 2mm, occurs as an interstitial phase in the anorthosite. Surrounding plagioclase is sericitizated. Ilmenite is altered to variable degrees to titanite, titanohematite and rutile (Fig. 10e–f).

7.2.4 Altered norite

Several samples which did not fit in Årebäck's (1995; 2001) descriptions of the island's bedrock were investigated. Investigations yield a primary mineralogy of plag+opx+cpx+ilm+mt±qz±ap±py. Secondary minerals are chl+hbl+bt+rut+tit+hem. The mineralogy classifies them as an altered noritic rock. Grain-size ranges from 2–6mm. Some samples have remnants of plagioclase megacrysts. These are either completely altered or show only an altered rims.

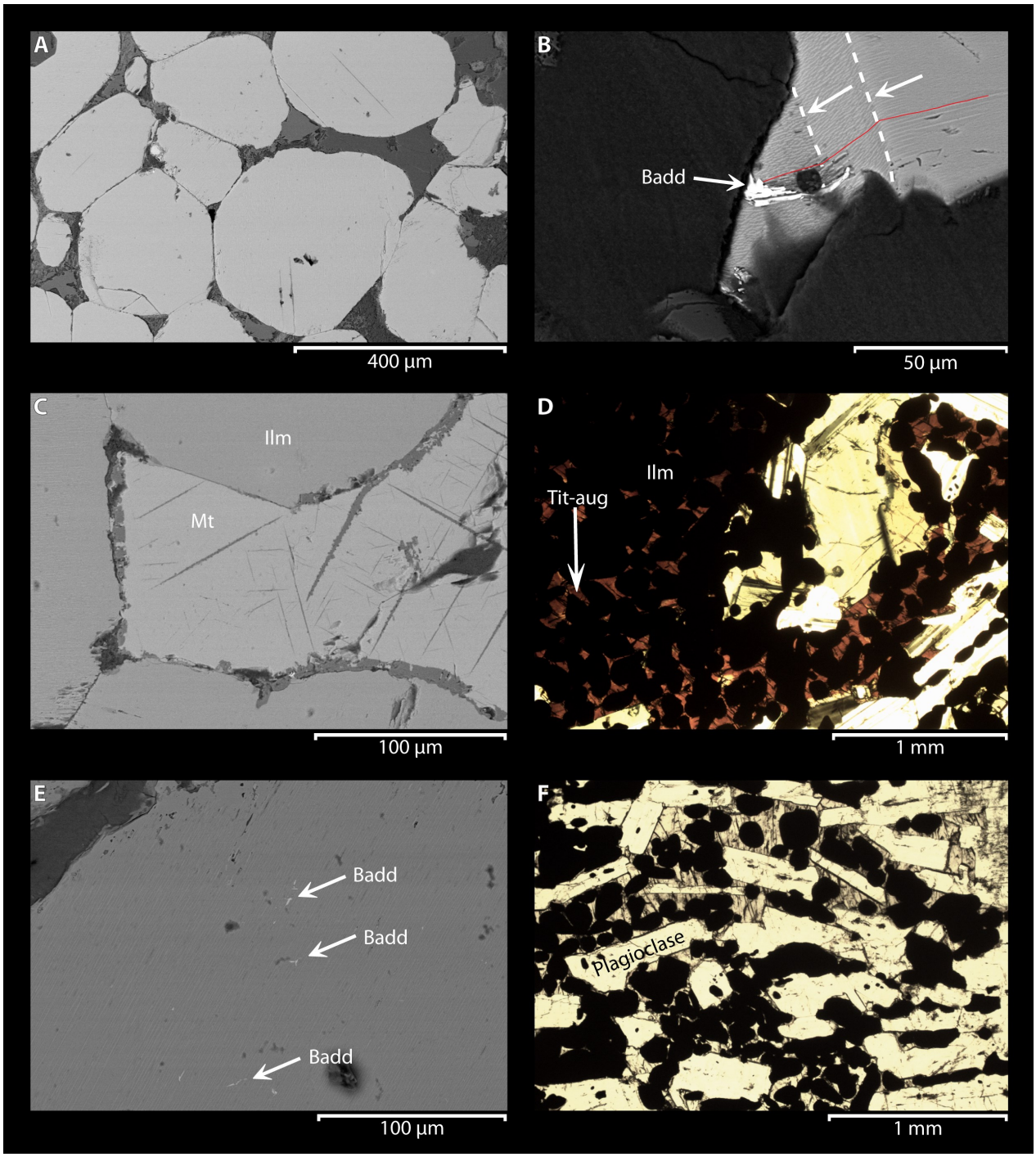

Fig. 9. Six pictures showing the main results for the IRL and its inclusions. *a)* Hematite exsolutions are so small that they are not visible in this picture but they are still there. *b)* Some grains of ilmenite have kink-bands, marked by arrows. If not for the hematite exsolutions (red line), the kink-bands would not have been visible. The bright phase is an inclusion of baddeleyite. *c)* In the picture two sets of trellis lamellae are visible within the magnetite. It was only possible to analyze the bigger set, which is ilmenite. When magnetite is occurring, it is as an interstitial phase to ilmenite. *d)* When clinopyroxene gets a substantial amount of titanium it becomes yellowish/reddish and is called titanaugite. The red phase is one single crystal of titanaugite, enveloping the ilmenite grains. *e)* Microscopic inclusions of baddeleyite often occur. It is not believed that they are exsolutions since they do not follow the same orientation as the hematite-exsolutions. *f)* Picture showing the relationship between ophitic plagioclase in the IRL-matrix and ilmenite. As seen the plagioclase have a general orientation which in field is W-E. Orthopyroxene and ilmenite occur as interstitial phases. © Sara Kullberg

Ilmenite occurs in three ways; discrete grains of ilmenite with oxidation-exsolution textures of rutile and titanohematite, ilmenite with alterations of titanite and ilmenite occurring as lamellae in titanaugite. The ilmenite lamellae have intersections of 120/60 degrees (Fig. 11a). Magnetite is either homogenous or has small Trellis lamellae. There are no reaction rims between ilmenite and magnetite. When the ilmenite has alterations of rutile, these are often more randomly oriented compared to the alterations of titanite that

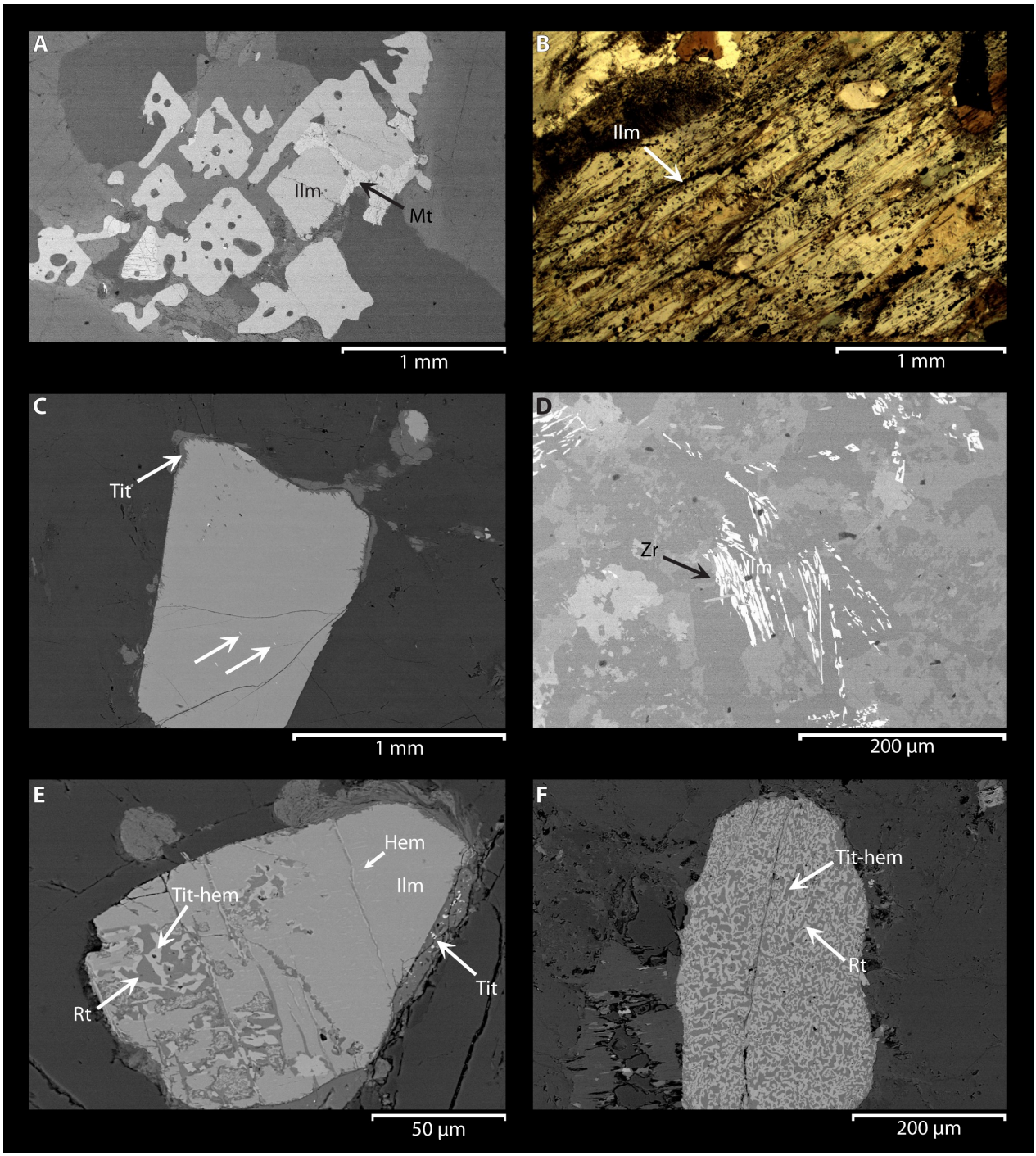

Fig. 10. Six pictures showing how ilmenite varied in appearance between the different lithological units. *a)* Skeletal ilmenite in contact with magnetite, found in norite samples. There is no reaction rim between the two oxides, which can be seen in other lithological units. *b)* Small grains of ilmenite lie as strings of pearls within pyroxene. The pyroxene is almost completely altered to chlorite and hornblende. It is possible that this sample should be classified as an altered norite, although assigned to a norite in this case. *c)* Ilmenite found within the monzonorite is quite homogenous with only some hematite lamellae and some inclusions of baddeleyite, indicated with arrows. Surrounded by a thin rim of titanite. *d)* Long, lath-shaped zircon occur throughout the sample. They overprint the primary mineralogy. It is the same sample as in picture c. *e)* The left-most part of the ilmenite has been altered to titano-hematite and rutile whereas the right-most part is quite homogenous with only some exsolutions of hematite. It is further rimmed by titanite. *f)* A grain of ilmenite has been completely altered to a complex intergrowth of titano-hematite and rutile. Both *e* and *f* are found as inclusions in the anorthosite. Although, similar textures are found in the monzonorite and the altered norite. © Sara Kullberg

tend to be more subparallel to each other. Ilmenite do not display either one type of alteration or the other, but often the two types of alterations occur within one single grain of ilmenite, see figure 11b. In some cases zircon rims the oxides (Fig. 11c).

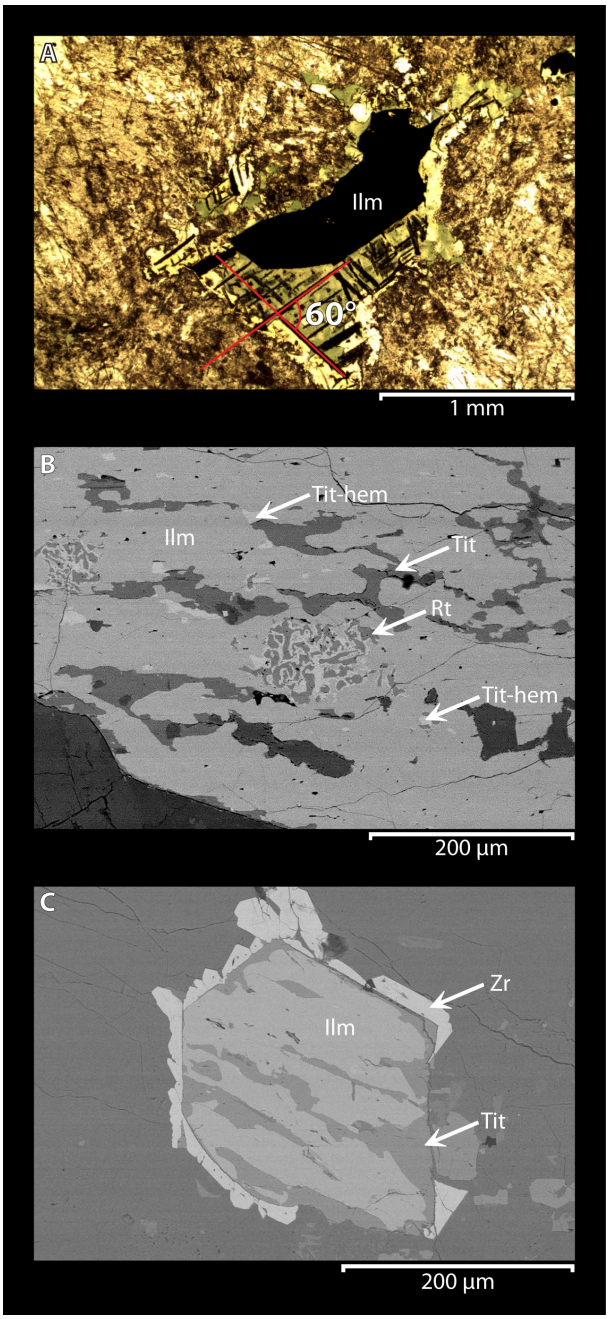

Fig. 11. The following pictures are all from an altered norite. As it is seen, *b* and *c* show many similarities to previous pictures. *a)* The sample is completely altered as seen by the mottled appearance. The ilmenite lamellae intersect at 60°/120° which is marked by a red cross. They occur in a dark green phase which is pyroxene that has been altered to amphibole. Only a few of these intergrowths were found. *b)* The titanite-alteration often follows a left-right trend, being sub-parallell to each other whereas rutile-titano-hematite intergrowths are more random in appearance. The two types of alterations can, as seen in this picture, occur together or independent of each other. *c)* Subhedral to euhedral grains of zircon rim the ilmenite. This particular grain exhibits titanite alterations only, which are also subparallel to each other. © Sara Kullberg

7.3 Field-relations

The magnetic veins have sharp contacts to the surrounding IRL-matrix and break up in angular fragments (Fig. 12a). The veins follow the same orientation as does the IRL-matrix. As opposed to oxide aggregates which can have diffuse borders, magnetic veins always occur as distinct inclusions (Fig. 12b).

Oxide aggregates show variable strength in magnetism when comparing with a hand-magnet. They are fine-grained and contacts to the matrix are somewhat diffuse, sometimes being gradual and sometimes sharp. Most often they consist of only oxides but occasionally small clusters of plagioclase in snowflake shape are visible. When occurring together, the change between them is gradual (Fig. 12c). Furthermore, some oxide aggregates show internal flow structures which are discordant to the flow structure in the IRL-matrix (Fig. 12d).

Anorthosite inclusions have sharp contacts to the matrix. They are not aligned to the E-W sense of flow defined by the IRL-matrix but more randomly oriented. Often a concentration of oxides is visible around the anorthosite (Fig. 13a), also marked by an increase in magnetism when testing with a hand-magnet.

When the concentration of the oxides increases in the IRL-matrix, the sense of flow decreases due to a relatively lower abundance of ophitic plagioclase. However, if there are more separate oxide aggregates the sense of flow becomes more visible due to their alignment with the sense of flow in the matrix.

Sugary anorthosites do sometimes occur as distinct inclusions with sharp contacts to the matrix, but sometimes the contact is gradual. Just like the coarse-grained anorthosite, these tend to have an oxide aggregate around them (Fig. 13b).

Laminated inclusions and the grey inclusions were small and not very abundant. Both had sharp contacts to the matrix.

The IRL-matrix itself is not homogenous regarding mineral distribution. Often there are mineral segregations where some domains are dominated by oxides and other by plagioclase (Fig. 13c).

7.4 Ilmenite composition

The results are summarized in figure 14. Figure 14a depicts the correlation between FeO and TiO_2. The majority cluster close around the reference point for pure ilmenite. The altered norite analysis cluster somewhat lower compared to the majority of the results, which is due to the fact that ilmenite in the altered norite is partly altered to titanite which is rich in Ca.

In figure 14b the Ca-component is added. The samples with the lowest Ca-content are those of the IRL and its mafic inclusions. Remaining points scatter along a trend-line, becoming increasingly rich in CaO.

FeO/TiO_2 against MgO or MnO show two trends (Fig. 14c–d). The former gives a bimodal distribution whereas the latter gives a gradual change. The most MgO-enriched is the snowflake-textured oxide aggre-

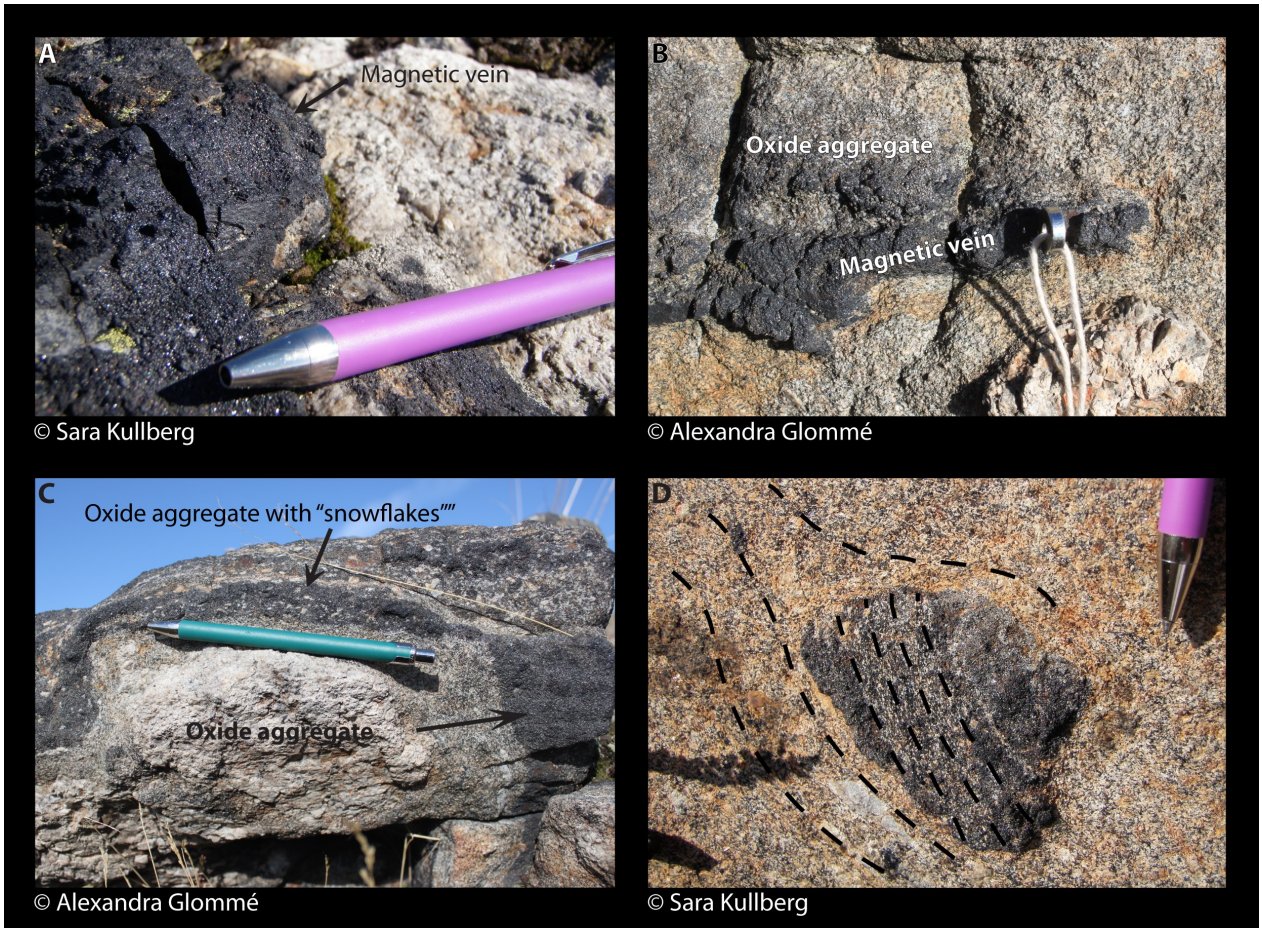

Fig. 12. a) The magnetic vein can either occur as an isolated inclusion within the IRL-matrix or in close association to anorthosite, such as in this picture. When occurring in great abundance it becomes visible that they break up in angular fragments. *b)* The magnetic vein protrudes out from the matrix to a greater extent compared to the oxide aggregate. *c)* The change between a pure oxide aggregate and an oxide aggregate with snowflake textured plagioclase is also gradual. They also occur in close association the anorthosite. *d)* Some oxide aggregate inclusions have an internal flow-structure, deviating from the flow-structure of the IRL-matrix. © Sara Kullberg

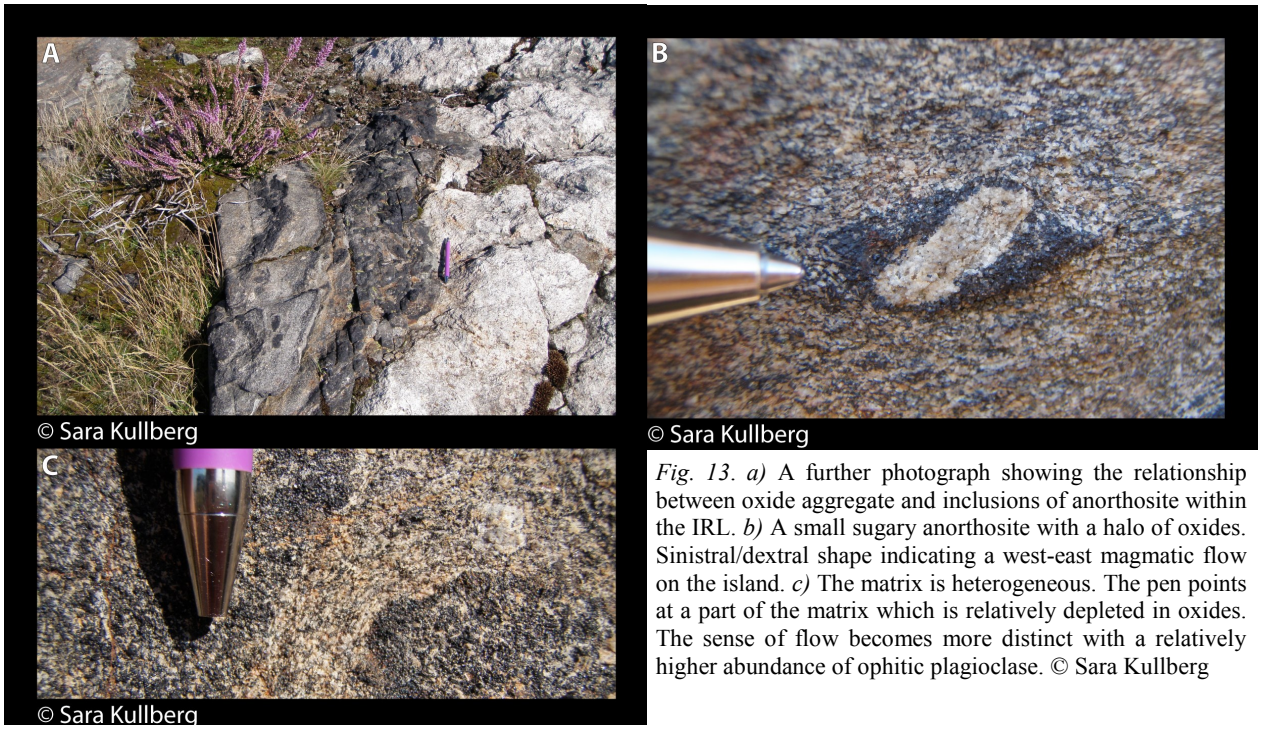

Fig. 13. a) A further photograph showing the relationship between oxide aggregate and inclusions of anorthosite within the IRL. *b)* A small sugary anorthosite with a halo of oxides. Sinistral/dextral shape indicating a west-east magmatic flow on the island. *c)* The matrix is heterogeneous. The pen points at a part of the matrix which is relatively depleted in oxides. The sense of flow becomes more distinct with a relatively higher abundance of ophitic plagioclase. © Sara Kullberg

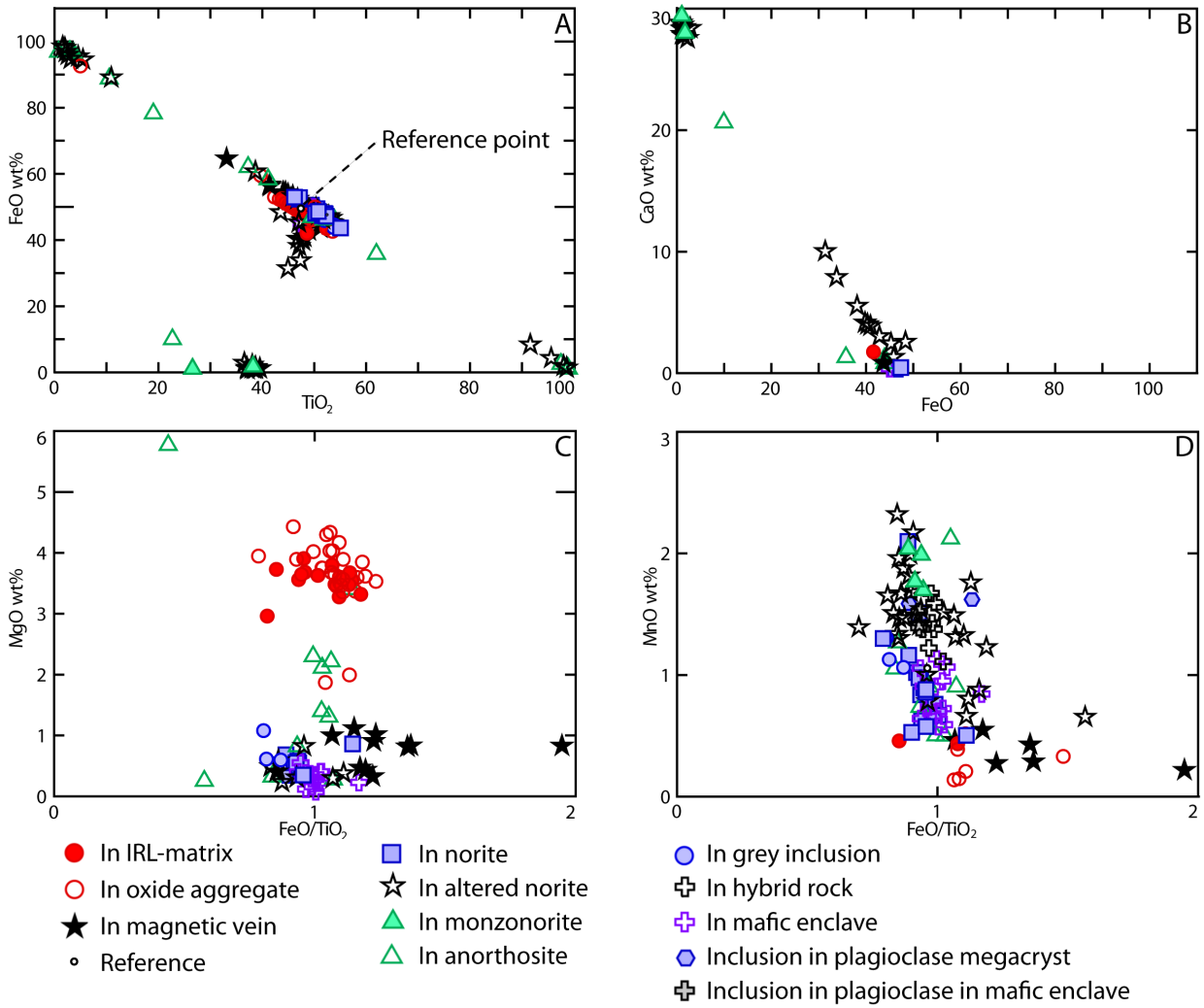

Fig. 14. The diagrams are based on data on ilmenite collected in SEM. *a)* The majority of the points cluster around the ratio 1:1 that is pure ilmenite. The points that deviate are alterations; 100% FeO is hematite, 100% TiO_2 is rutile and titanite is 30-40% TiO_2 and 0% FeO. *b)* It is mainly the altered norite and the monzonorite that has titanite-alterations as seen in higher % of CaO. Some samples are more altered compared to others. *c)* The lithological units are divided into relatively Mg-rich and Mg-poor. The IRL is in general more Mg-rich apart from the magnetic vein which is poor in MgO. *d)* The change in Mn-content is gradual. The Mn-component in ilmenite is more gradual. Here all the IRL components cluster around the same Mn-content.

gate, followed by the IRL-matrix and the oxide aggregate. The ilmenite occurring as inclusions in the anorthosite have variable values for both MgO and MnO.

7.5 Bulk rock data

The following figures are all based on the bulk rock data given in appendix IV. Firstly, by plotting FeO-TiO_2 two trends become visible. The norite and the altered norites show a more iron-enriched fractionation trend; whereas the IRL and its inclusions show a more 1:1 FeO-TiO_2 fractionation trend (Fig. 15a).

When depicting the relationship between MnO and FeO/TiO_2 in figure 15b, it is notable that the IRL-samples all lie on FeO/TiO_2=1 whereas the altered norites have higher ratios. The IRL-samples are richer in MnO compared to the altered norites.

Spider-diagrams of the REEs (Rare Earth Elements) show that all units are somewhat parallel to each other (Fig. 15c). The norite, mafic enclave and monzonorite all show negative europium anomalies, whereas the IRL-matrix, the magnetic vein and one sample of the altered norites show positive europium anomalies. The slope is overall negative, apart from a few HREE (Heavy-REE) which show a positive slope.

Figures 15d–e show trace element plots. As seen in the figures the IRL is more depleted compared to the norite and the altered norite, apart from Ti which is highly enriched in the IRL due to ilmenite. Within the IRL, the magnetic vein is the least enriched and the IRL-matrix, the most. The norite and the altered norite show the same signature, even though the altered norite displays many secondary phases.

7.6 AFC model

The model is based on trace elements, listed in appendix IV, and their distribution coefficients, listed in appendix V. The data collected from the norite provide values for C_m and data from the SLM provide values for C_a. The results are visible in figure 16.

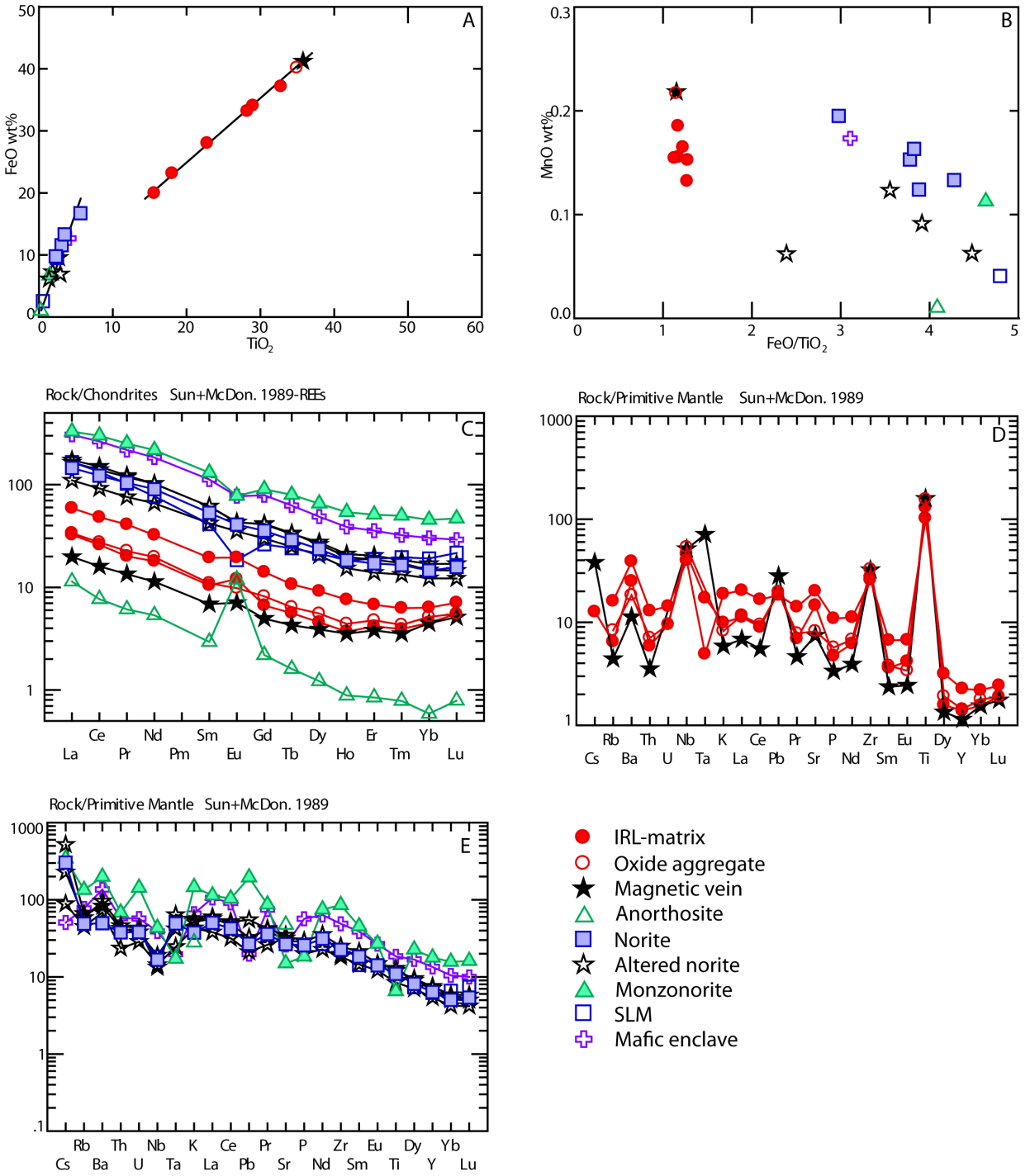

Fig. 15. Five plots summarizing the main results for the Hakefjorden Complex. *a–b* only depict main element trends whereas plots *c–e* depict trace element trends. *a)* Two trends become distinct when plotting FeO against TiO_2. The reason behind the more Fe-enriched trend in the norite, altered norite and monzonorite is discussed later on. *b)* When looking at bulk rock data, the IRL and its inclusions are slightly more enriched in Mn. The other lithological units are more enriched in Fe as seen in the higher FeO/TiO_2 ratio. *c)* REE-data show a negative trend for the LREE but either a horizontal or positive trend for the HREE. The anorthosite, and to some extent the IRL and its inclusions, have a positive Eu-anomaly due to cumulative plagioclase. *d)* The IRL, the oxide aggregate and the magnetic vein all display the same positive anomalies due to their similar mineralogy. *e)* The norite and the altered norite display similar patterns. Note that they lack negative anomalies for which the IRL has positive anomalies.

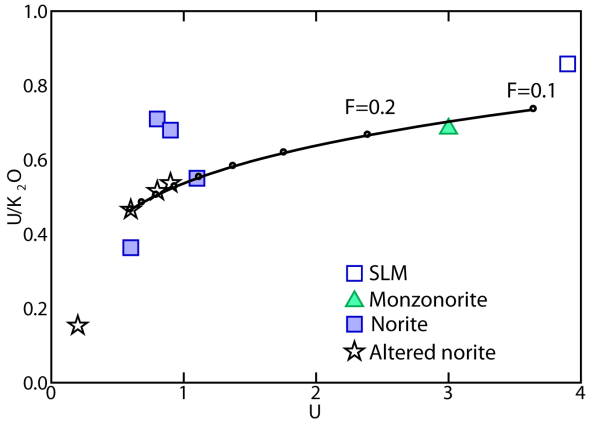

Fig. 16. A plot showing the relationship between U/K_2O and U for the altered norite, norite, monzonorite and SLM. The IRL-unit is excluded from the plot since it is believed that it is not affected by contamination by the SLM. The black line represents the iteration made in IgPet, and its r-value is 0.05 which indicates limited contamination. Furthermore, contamination happened late in the crystallization sequence with only 10-20% of the magma remaining (F=0.1-0.2).Values were set at D_U=0.03 and D_{K2O}=0.25 based on D-values listed in appendix I and the relative abundance of phases seen in thin-sections.

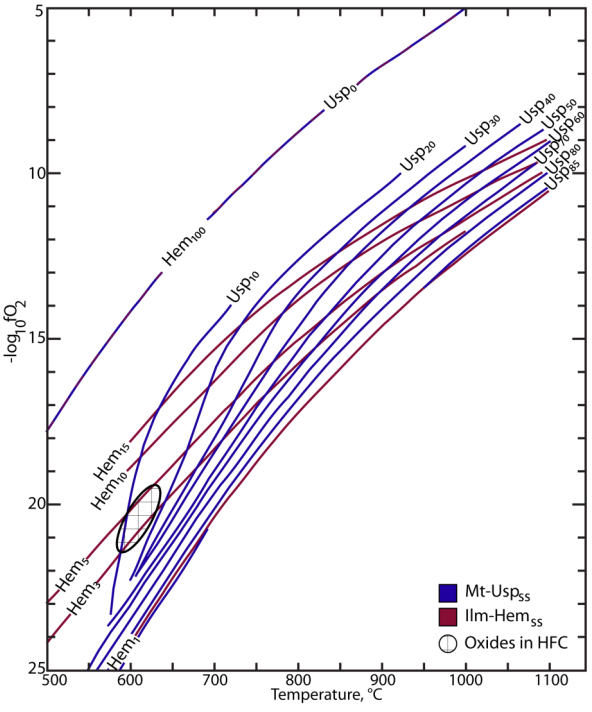

Fig. 17. As it was assessed that the Usp-component varied between 10–20 wt% and hematite between 3–10 wt%, due to the low visibility of hematite exsolutions, the intersection between the phases was rather low. Temperatures varied between 550°C and 650°C and oxygen fugacities $-\log fO_2$ 19 –22. Modified after Buddington and Lindsley (1964).

7.7 Temperature and fO_2

The hematite component of ilmenite was estimated to be low (≈3–10 wt%) due to low visibility in optical microscope. The ulvöspinel component was calculated to be 10–20 wt% based on weight % TiO_2 in the magnetite. Since no disequilibrium textures were found among the Fe-Ti oxides it is believed that they are in equilibrium. Hence, the intersection between Mt-Usp$_{ss}$ and Ilm-Hem$_{ss}$ in figure 17 is thought to represent the temperature and oxygen fugacity of the time of formation.

8 Discussion

Petrographic studies show textural differences in the oxides between the different petrographic units, as seen in figures 9–11. The variance in textural appearance of the oxides is interpreted to indicate changes either in P/T-conditions or as indicative of changes in fO_2 as a result of fluids. Textural variance due to changing P/T-conditions can give an indication of crystallization sequence of the lithological units.

As previously described, the hematite content and ulvöspinel content of the ilm-hem$_{ss}$ and mt-usp$_{ss}$, respectively, increase with increasing temperature (Lindsley 1991). Comparing the magnetite in the IRL and its inclusions, and the norite it is notable that the magnetite in the former has been exsolved to a higher degree. This would indicate a relatively higher ulvöspinel component in the IRL and hence an earlier formation compared to the norite. Microprobe analysis shows that the magnetite in the IRL has a relative enrichment in TiO_2.

It was possible to determine relative ages by looking at magnetite, but the same is not possible for ilmenite. The hematite content does not change drastically with increasing temperatures, as seen in figure 2.

Fluid induced textures were found in the altered norite, the monzonorite as well as in the anorthosite. Ilmenite-lamellae in magnetite were altered to titanite, the pyroxenes have undergone biotization and the feldspars, seritization which all are strong indications that fluids have been involved. These textures are thought to belong to a late stage magmatic fluid event.

In comparison to magnetite, ilmenite has more complex oxidation textures. Either the ilmenite had become replaced by an intergrowth of rutile and titanohematite (step R4) or ilmenite+titanite, with titanite either as lenses within the ilmenite or as coronas around it, see figures 10d–f and 11b–c.

Sometimes the two types of intergrowths occur within one single grain. As the different oxidation textures have different requirements regarding fluid chemistry, either there has been two generations of fluids, or the chemistry of the fluid has changed during its course throughout the lithological units. Either way, the deuteric oxidation is a late magmatic event.

Magnetite, if rich in the ulvöspinel component, can form the same rutile-titano-hematite pattern observed in the samples (Haggerty 1991, this thesis). As stated

by Årebäck and Stigh (2000), as well as seen in the results of this study, the ulvöspinel component is poor in magnetite and it has therefore been rejected that the fluid induced textures are a result of oxidation of primary magnetite.

To summarize: textures, found in the magnetite and ilmenite, provide evidence that the IRL crystallized before the norite. Furthermore, a fluid event has altered the oxides. The alteration is thought to be a late stage magmatic event. This interpretation is in accordance with results from major element analysis of the oxides.

8.1 Fe-Ti oxide chemistry

Ilmenite from the altered norite and monzonorite are richer in manganese compared to ilmenite in the norite, IRL and anorthosite (Fig. 14d). The compatibility of manganese in ilmenite is temperature dependent; the colder it is the more manganese it incorporates (Lindsley 1991; Charlier et al. 2007). This would imply that the altered norite and the monzonorite actually crystallized at lower temperatures compared to the rest of the complex. Although, the gradual change in manganese-content indicates that the bedrock units crystallized rather continuously. Interestingly the IRL and its inclusions show the lowest Mn-content indicating that the IRL, and especially the magnetic vein, pre-dates the norite and the monzonorite. The Mn-content in ilmenite found as inclusions within the anorthosite indicate that the anorthosite began to crystallize simultaneously with the IRL and continued to crystallize together with the norite.

IRL bulk rock data yield that the IRL is the most enriched in MnO. This is likely an effect of accumulation of manganese-bearing minerals, and the individual grains themselves are in fact depleted in MnO compared to ilmenite found in the altered norite.

Furthermore, the MgO-content of ilmenite has a bimodal distribution with the ilmenite in the IRL-matrix and oxide aggregate being enriched in MgO and the magnetic vein being depleted in MgO. The norite, altered norite and monzonorite are also depleted in MgO (Fig. 14c). Årebäck (2000) hypothesizes that the difference in MgO-content is due to re-equilibration between oxides and silicates. This does not comes to terms with the relationship depicted in figure 12b. Here an oxide aggregate (MgO-rich) lies close to the magnetic vein (MgO-poor). As the oxide aggregate has a higher modal abundance of silicate phases it should be this unit that is MgO-poor and not the other way round. The amount of phosphorous, P_2O_5, in the melt might explain this trend. High concentrations of P_2O_5 inhibits MgO incorporation into ilmenite (Charlier *et al*. 2007). At the same time it also destabilizes the crystallization of magnetite (Toplis *et al*. 1994). As the magnetic vein is rich in magnetite, this becomes contradictory. It could be theorized that there have been several magma batches, although with the same origin due to consistency in $^{87}Sr/^{86}Sr$, with different saturations in P_2O_5. The magnetic vein could therefore be theorized to be an autoxenolith, crystallized early but from another batch of melt.

Two crystallization trends are visible in figure 15a where the two sets (IRL vs. the rest) have different slopes. The IRL and its inclusions have a less steep slope compared to the other units, almost with a k-value of 1 indicating crystallization of ilmenite. The others show a more iron-enriched slope. This could be explained by crystallization of pyroxenes alongside the ilmenite. Nevertheless, the change in the slope point to a change in which phases co-crystallize which is probably due to cooling of the system and decompression.

To summarize: Mn-data on ilmenite indicate that the IRL predates the anorthosite, followed by the norite and lastly the monzonorite but that crystallization was rather continuous. The bimodal Mg-trend is an artifact of oxide-silicate re-equilibration. Finally, the contrasting slopes are a result of changing crystallizing phases.

8.2 Trace elements

Incompatible trace elements were plotted (Fig. 15d–e). The IRL and its inclusions show distinctive positive peaks for Ba, Nb, Pb, Sr, Zr and Ti. This can be explained by the fact that Ba, Pb and Sr are all compatible in plagioclase and Nb, Zr and Ti are all compatible in ilmenite (Winter 2009). As the IRL is a cumulate (Årebäck 1995) these elements become relatively enriched, resulting in positive peaks. Since Årebäck (2001) stated that the norite is also a cumulate, it would be expected to find the same peaks as in the IRL due to similar mineralogy. Although, this is not visible in the results of this study. As previous discussion has elucidated, the IRL formed prior to the norite, which could have led to a depletion of certain trace elements in the remaining magma. The norite and the altered norite do not show the correlative negative anomalies for Ba, Nb, Pb, Sr, Zr and Ti. This either implies that the norite is not the parent for the bulk IRL and its inclusions, or that the crystallization of the IRL did not affect the remaining magma due to mass balance. Nevertheless, the norite and altered norite do show weak negative anomalies for Nb, Pb and Zr which could be accounted for by some fractionation of ilmenite and plagioclase. Additionally, figure 15c depicts the REE curves for all the lithological units. It shows that the IRL is less enriched than the monzonorite. Once again, data indicate that the monzonorite is the most evolved unit and the IRL the least evolved unit.

$FeO\text{-}TiO_2$ shows two crystallization trends (Fig. 15a), a plot of La/YbN-Yb shows the same trends with two contrasting slopes (Fig. 18). The IRL and its inclusions have a steep slope whereas the rest lie on a horizontal line. One possible explanation behind this phenomenon is the titanaugite (clinopyroxene) found as a poikilitic phase in the IRL. Titanaugite has a higher partition coefficient for the HREE compared to the LREE. With fractional crystallization the ratio La/Yb in the remaining liquid increases as the relative

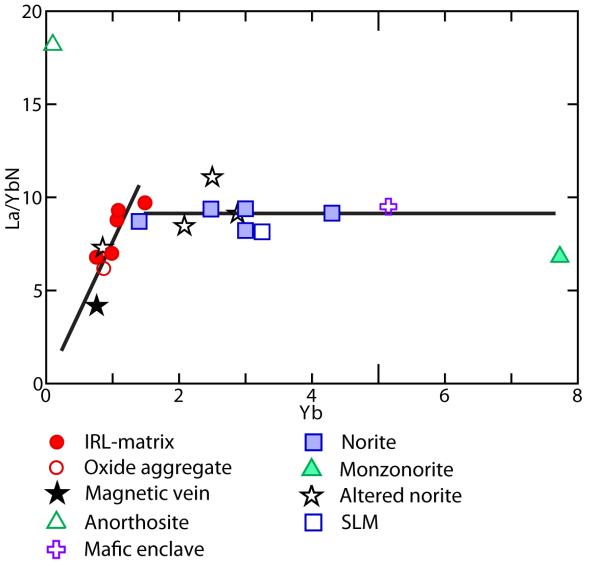

Fig. 18. The more Yb-enriched the sample is, the more evolved it is. As seen in the diagram the monzonorite shows the most enriched trend, whereas the magnetic vein shows the most primitive signal. This is further evidence that the magnetic vein is the earliest formed unit and the monzonorite is the last formed unit.

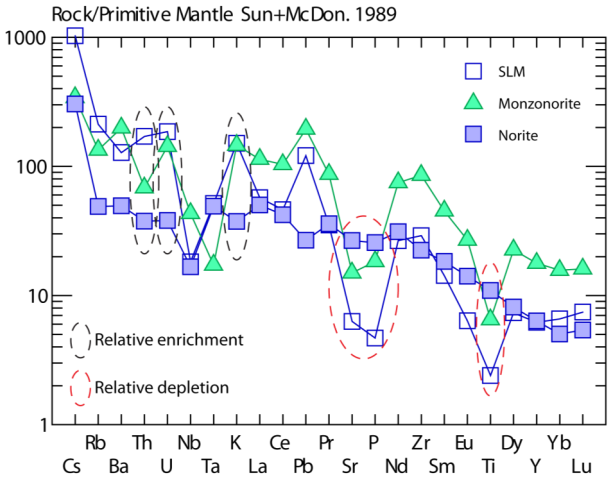

Fig. 19. As it is seen in the figure monzonorite more or less parallel the norite, although more enriched. Elements that deviate are encircled either in blue or red. Blue indicates that the monzonorite has become enriched by the SLM contamination and red indicates that it has been relatively depleted by the contamination. Th, U and K are relatively enriched and Sr, P and Ti are relatively depleted. Elements that are most enriched in the SLM, least enriched in the norite with the altered norite somewhere in between have been used in the AFC-modeling.

amount of Yb compared to La, decreases. This in turn would also indicate that the magnetic vein was the first unit to form due to its low Yb and La/Yb. Thereafter the oxide aggregate crystallized and lastly, the IRL-matrix. Later on in the crystallization sequence, the norite and the altered norite crystallized. As they crystallized the La/Yb was fixed and further crystallization seemingly did not affect the ratio, probably as an effect of decreasing crystallization of titanaugite. Monzonorite was the last unit to crystallize, as evident by the La/YbN-Yb plot (Fig. 18).

Crystallization of titanaugite in the IRL with its relatively higher affinity for the HREE would explain the positive HREE slope (Fig. 15c). Normally, partial melting of a source rock and subsequent crystallization will result in a negative slope of the REEs (Winter 2009). In this case, the IRL is a cumulate where the HREE will be incorporated to a higher extent compared to the LREE due to the higher distribution coefficient of the HREE (appendix V), thus making the slope positive. The positive slope is then not a signal of the magma source, but the result of fractional crystallization.

As it is assumed that the SLM has contaminated the Hakefjorden Complex (Årebäck 1995; this thesis) it seemed proper to compare the SLM, monzonorite and norite in a spidergram of incompatible trace elements (Fig. 19). There are troughs for Ti, P and Sr in the monzonorite but as ilmenite, apatite and plagioclase are all present phases, the troughs cannot be accounted for by absence of these key minerals. The SLM, on the other hand, is depleted in these elements and troughs in the monzonorite are most likely a result from dilution by the SLM. The peaks in the monzonorite of U, K and Pb are then in fact a result of enrichment by the SLM. As the majority of the remaining trace elements are compatible in either crystallizing phase the only possible elements for modelling AFC are Pb, K and U. Without the relative dilution and enrichment of the monzonorite by the SLM it is plausible that the curve for monzonorite would parallel the norite, although somewhat more enriched reflecting only fractional crystallization.

To summarize: REE and trace element data all point at the magnetic vein within the IRL being the least evolved unit in the Hakefjorden Complex, and the monzonorite being the most evolved unit in the system. Once again, diverging slopes of trace elements ratios show that the liquid line of descent has changed during cooling of the magma.

8.3 AFC-model

The AFC-model was made in order to estimate to what extent fractional crystallization and contamination have affected the Hakefjorden Complex. There is some contamination made evident by the troughs and peaks in the monzonorite, inherited from the chemical signature in the SLM. Additionally, field-relations of the lithological units with monzonorite occurring as an outer rim in contact to the SLM strongly suggest contamination (Årebäck 1995). The modeling results show that the contamination is very small (Fig. 16). The only iteration that produced a result that fit the Hakefjorden Complex data was for an r-value of 0.05. Additionally, $^{87}Sr/^{86}Sr$ values are similar throughout the complex which is indicative of no or restricted contamination (Glommé 2015). Although, it cannot be ruled out that contamination and subsequent homoge-

nization have occurred prior to all crystallization. This is in fact a drawback of the model, which assumes that the SLM is the only rock that has acted as the contaminant. It could be that other rocks have contaminated during ascent of the magma.

Nevertheless, results herein show that the contamination by the SLM has been very small (r=0.05) and only affected the outer rim of the Hakefjorden Complex. The IRL is not taken into account since it has been concluded herein that it pre-dates the norite and was probably already crystallized at the time of contamination by the SLM.

Furthermore, the model does not take into consideration the partition coefficients of the SLM contaminant. The model only takes into account the concentration of one element in the contaminant. Depending on the partition coefficient of an element between a mineral in the SLM and the melt, the absolute concentration varies. The amount of melt produced also plays a role in the final concentration of the element which contaminates (Fig. 3).

Finally, as seen from previous results (Fig. 15a, 18) the rock units are divided into two trends, which can be accounted for by changes in mineral crystallization order. Only the final, cumulative result of crystallization is seen in thin section and it is this final ratio between phases that is used when generating the AFC model. The ratio has most likely varied and the effect of contamination likewise, therefore the result from the AFC model is very simplistic, taking only the final result into consideration.

To summarize: modeling in IgPet indicate that contamination is a minor process with the ratio Assimilation:Fractional Crystallization reaching 0.05. Due to drawbacks of the software this result should be treated with precaution. Nevertheless, $^{87}Sr/^{86}Sr$ values are similar throughout the units, supporting the hypothesis of restricted contamination (Glommé 2015).

8.4 Magma source

Since the results show that the units have different enrichment-trends it is appropriate to test whether the lithological units are all related or not. One way to do so is to plot the ratio of two incompatible elements against an incompatible element. Ce/Nd against Ce can be seen in figure 20. The ratio remains constant since neither Ce nor Nd are compatible in crystallizing phases (Winter 2009), see appendix V. The only exception is apatite where Ce is compatible. The effect of apatite is negligible in most samples. Although some samples show elevated Ce/Nd-concentrations which can be accounted for by crystallization of apatite (Fig. 20). As noted, the Ce/Nd for the SLM is similar to that of the Hakefjorden Complex, which could prove problematic. The same Ce/Nd could indicate that the Hakefjorden Complex has undergone massive contamination by the SLM and homogenized. On the contrary, two pairs of incompatible trace elements plotted against each other (Th/La vs. Sm/La) shows contrasting results for the SLM and the Hakefjorden

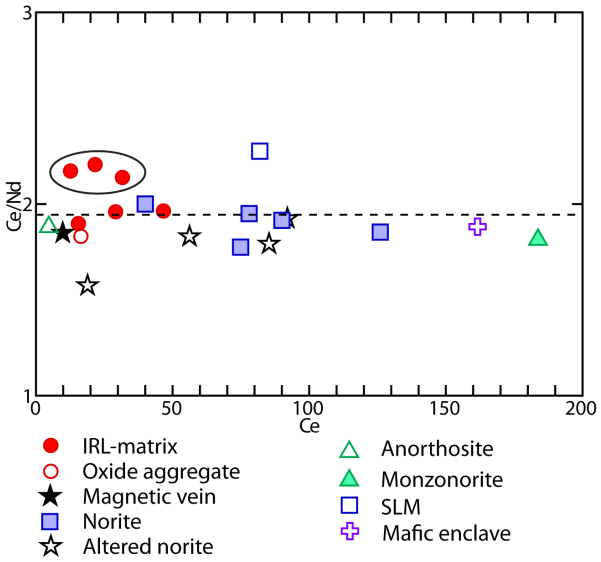

Fig. 20. All the units in the complex plot at a horizontal line when plotting Ce/Nd-Ce, indicating that they all stem from the same source with increasing fractionation to the right. Hence the magnetic vein and the anorthosite are the most primitive and the monzonorite is the most evolved. It could be that the elevated Ce/Nd values for the encircled points are due to accumulation of apatite.

Complex (Fig. 21a). Thus, that the SLM and the Hakefjorden Complex had the same Ce/Nd is just a coincidence. Trace element ratios are in accordance with the inference that all the units in the Hakefjorden Complex stem from the same source.

8.4.1 Continental crust or mantle?

The origin of Proterozoic massif type anorthosite complexes has long been debated (Ashwal 1993) and a final answer is not provided herein. The general belief has long been of a mantle derived melt that pools at the mantle-crust boundary where it begins to crystallize. The magma thereafter intrudes at mid-crustal levels where it is contaminated by crustal material (Longhi *et al*. 1999). Results from Longhi *et al*. (1999) show that in order to crystallize an anorthosite with related rocks from a mantle source; the ratio between assimilated granitic material and magma must have reached at least 0.2. Crustal contamination does not appear to be a major process in the Hakefjorden Complex, as seen in the AFC-model. The only option is if the Hakefjorden Complex has been contaminated early and homogenized throughout. It is not possible within the scope of this thesis to assess whether this has occurred or not.

When comparing the data generated in this thesis with data from ocean island arcs and continent island arcs (Fig. 21b, GeoRoc 2015) it becomes visible that the data for the Hakefjorden Complex plots somewhere in between an ocean island arc setting and a continental island arc setting. Additionally, pyroxene with ilmenite lamellae, indicative of high pressure (Wyatt 1977), were found in one sample (AGSKSE04). Even though this is indicative of a mantle source, REE-concentrations are too high to be in

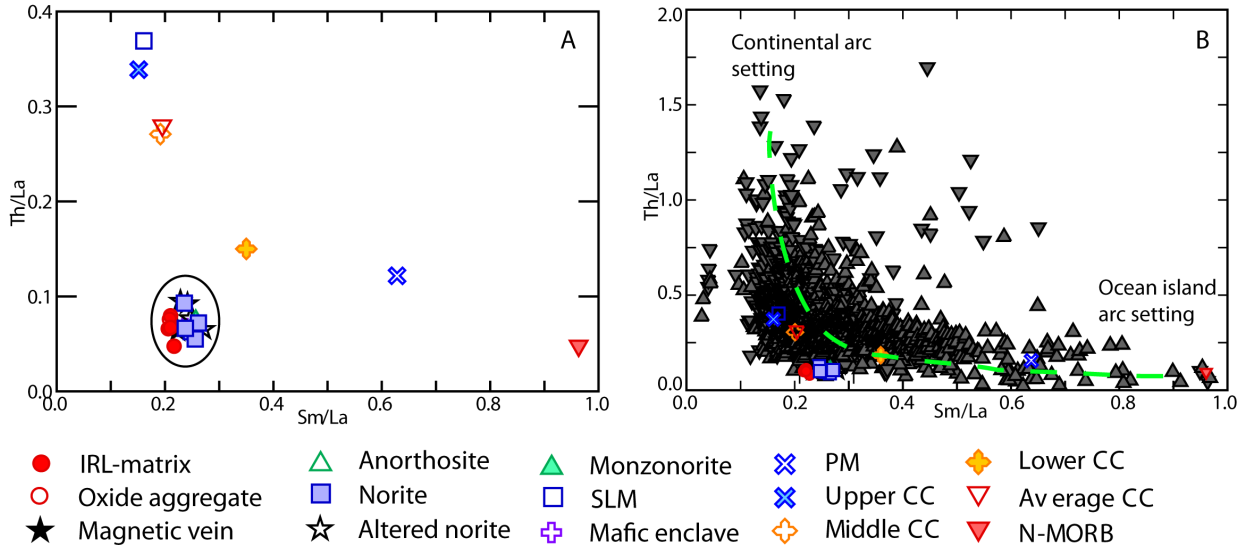

Fig. 21. a) When plotting the relationship between two ratios of incompatible trace element pairs it becomes obvious that the signal of the Hakefjorden Complex is homogenous. The SLM has a higher Th/La ratio and does not seemingly affect the ratio in the Hakefjorden Complex, indicating that contamination by the SLM is low. The data is closest to that of Lower continental crust (Lower CC). *b)* When plotting the Hakefjorden Data together with data from subduction settings, ranging from ocean island arc setting (close to N-MORB) to continental arc setting (high Th/La), the data plots in an intermediate setting. Data from Georoc.com (2015).

accordance with this. The double-dip of Ta and Nb is indicative of a subduction zone due to their relative similarities (Winter 2009). This double-dip does not exist in the data of the Hakefjorden Complex; the dip in Nb can be accounted for the crystallization of ilmenite. Nevertheless the source could still be a mantle enriched by fluids. Although, results from Vidal *et al.* 1989 show that a mantle source that have been metasomatically altered (thus enriched) have a U-shaped trace element pattern due to enrichment of LIL's (Light Ion Lithophiles), which trace element data in this thesis do not display. Furthermore, data from an enriched mantle never exceeded 10 times that of CHUR (CHondritic Uniform Reservoir, Vidal *et al.* 1989) compared to results herein, which exceeds CHUR 10 to 100 times (Fig. 22). Hence, it is not likely that the source for the Hakefjorden Complex is neither a depleted mantle nor an enriched one.

Finally, Sr-isotope data from Glommé (2015) indicates a crustal source. Since Th levels are low, it is not possible that the source is upper crust but rather a lower, mafic crust that has not been enriched in Th. Re-Os data of the Rogaland province and indicate that the origin is a mafic lower crust (Schiellerup *et al.* 2000). As the Hakefjorden Complex displays many similarities to the Rogaland anorthosite province, both chemically, geographically and in age, it might be possible that it shares the same magmatic origin as well.

8.5 Summary - a general model

Main element data, as well as trace element data, all point toward units forming in the following chronological order; from oldest to youngest; magnetic vein → oxide aggregate (with or without "snowflakes") →

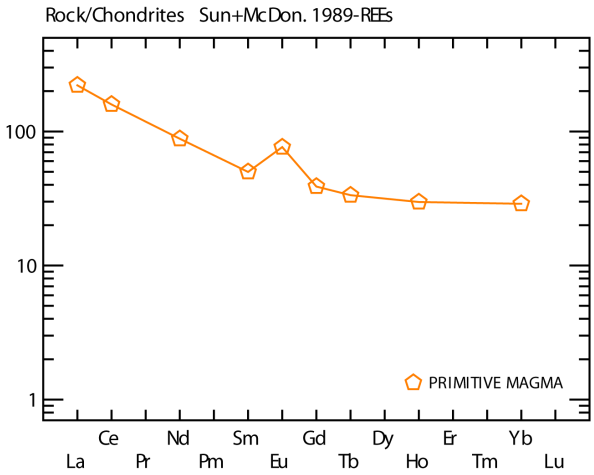

Fig. 22. As results have shown that the magnetic vein is the most primitive unit of the Hakefjorden Complex, the magnetiv vein is also the unit which has been in equilibrium with the primitive magma. The REE-pattern for the most primitive magma was calculated by dividing the concentration in the magnetic vein with the distribution coefficient for each element, as done by Simmons and Higgins (1978). As seen in the figure the trend is highly enriched. Furtherore it displays a small positive europium anomaly which can be accounted for by some accumulation of plagioclase.

IRL-matrix → anorthosite/norite → norite/altered norite → monzonorite.

The anorthosite formed in a deep seated magma chamber before rising to its emplacement depth (Årebäck & Stigh 1997), the IRL and its inclusions also formed in a deep seated magma chamber, more or less contemporaneous with the anorthosite.

This chronological order is problematic as norite is found as inclusions within the IRL, and monzonorite as inclusions in the norite (Årebäck 1995; Årebäck &

Stigh 2000). These relationships imply the opposite chronological order. One way to explain it is by looking at the IRL as a not completely solidified crystal mush when rising towards it final emplacement depth (Fig. 23). Along the way, norite started to crystallize and blocks became incorporated to the not yet completely solidified IRL. As the complex rose to its final depth the core consisted of partly solidified material. Surrounding it was anorthosite floating in suspension in a still hot norite. As the central parts already were partly solidified, the rest of the magmatic system crystallized from the inside and out and thereby explaining as to why the monzonorite is the most enriched unit. Alternatively, there have been several batches of magma with slight differences in composition mixing.

The magmatic system was obviously dynamic as seen in flow structures within the IRL, but also in the anorthosite (Fig. 24). It is therefore not impossible that the entire complex has rotated around a solid center.

Furthermore, equilibria between magnetite and ilmenite also show at what temperature and oxygen fugacity the units crystallized. As seen in the results the temperatures vary between 500–650°C. As the temperature of emplacement has been estimated to 890 –1015°C (Årebäck & Andersson 2002) this temperature is unlikely. Furthermore, Årebäck and Stigh (2000) concluded with help of pyroxene-equilibria that the crystallization temperature was in the regime of approximately 1000–1100°C, with the IRL crystallizing in the upper end and the norite in the lower end. Rather the temperature calculated here indicates a re-equilibration temperature. As theorized by Årebäck and Stigh (2000) the textural appearance of the ilmenite in the IRL is indicative of post-crystallization modification (Årebäck & Stigh 2000). Re-equilibration would indicate mass transport, off-setting geochronological trends seen in the textural appearances of the oxides. But as temperature estimates from Årebäck & Stigh (2000) combined with trace element data in this report still indicate that the IRL pre-dates the rest of the Hakefjorden Complex, it is believed that the re-equilibration has not significantly affected the oxides and that the trends seen in textures and main elements are still applicable.

8.6 What remains to be done?

Although many questions have been answered within this thesis, many questions still remain. The U-Pb dating of a zircon found in a granitic contact melt yielded an age of 916±11 Ma (Scherstén *et al.* 2000). When taking into consideration that a dyke of the Göteborg dykes (935±3Ma) crosscut the monzonoritic zone at Brattön (Årebäck 1995; Hellström *et al.* 2004), this age cannot be interpreted as the age of the intrusion. Further shortcoming is that the age estimation is from a contact melt and not the intrusion itself. As it probably took some time for the melt to form and subsequently crystallize, the age-estimate from this is probably younger than the Hakefjorden Complex itself. It could also be that the age of the monzonoritic dyke is

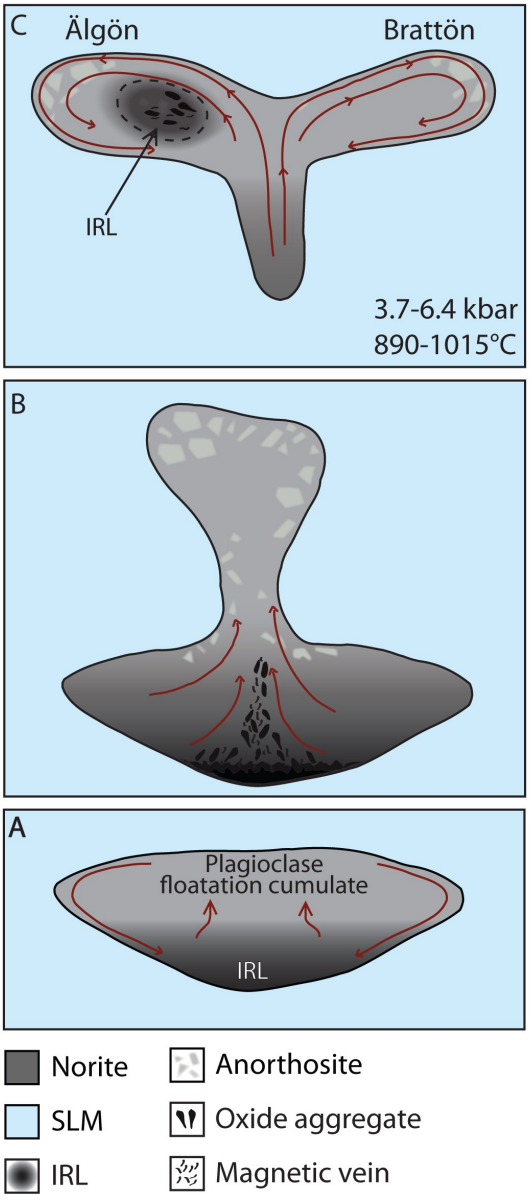

Fig. 23. A new model that adds new information to the model made by Årebäck and Stigh (1997, Fig. 8). The IRL is in this model an early formed cumulate, possibly contemporaneous to the anorthosite. *a)* In the deep-seated magma chamber magnetite and ilmenite-saturated material start to settle, forming the magnetic vein and the oxide aggregate. Although, the magnetic vein might an autoxenolith, originating from an even earlier phase in magma crystallization. Simultaneously plagioclase crystals form a floatation cumulate at the roof of the magma chamber. *b)* When the magma starts to migrate upwards the IRL-units are disrupted and brought along. During ascent, the magma continue to crystallize and the IRL-matrix starts to form and the IRL with its inclusions become a semi-consolidated mush. *c)* During the final emplacement the IRL-mush was placed in the central parts of the island whereas the anorthosite gathered at the rims. As hot magma continued to pump up from below a the semi-consolidated core was enveloped in rotating hot material. This is theorized to be the reason of how the island has cooled from the inside and out as the geochemical analysis indicate. Modified after Årebäck (1995).

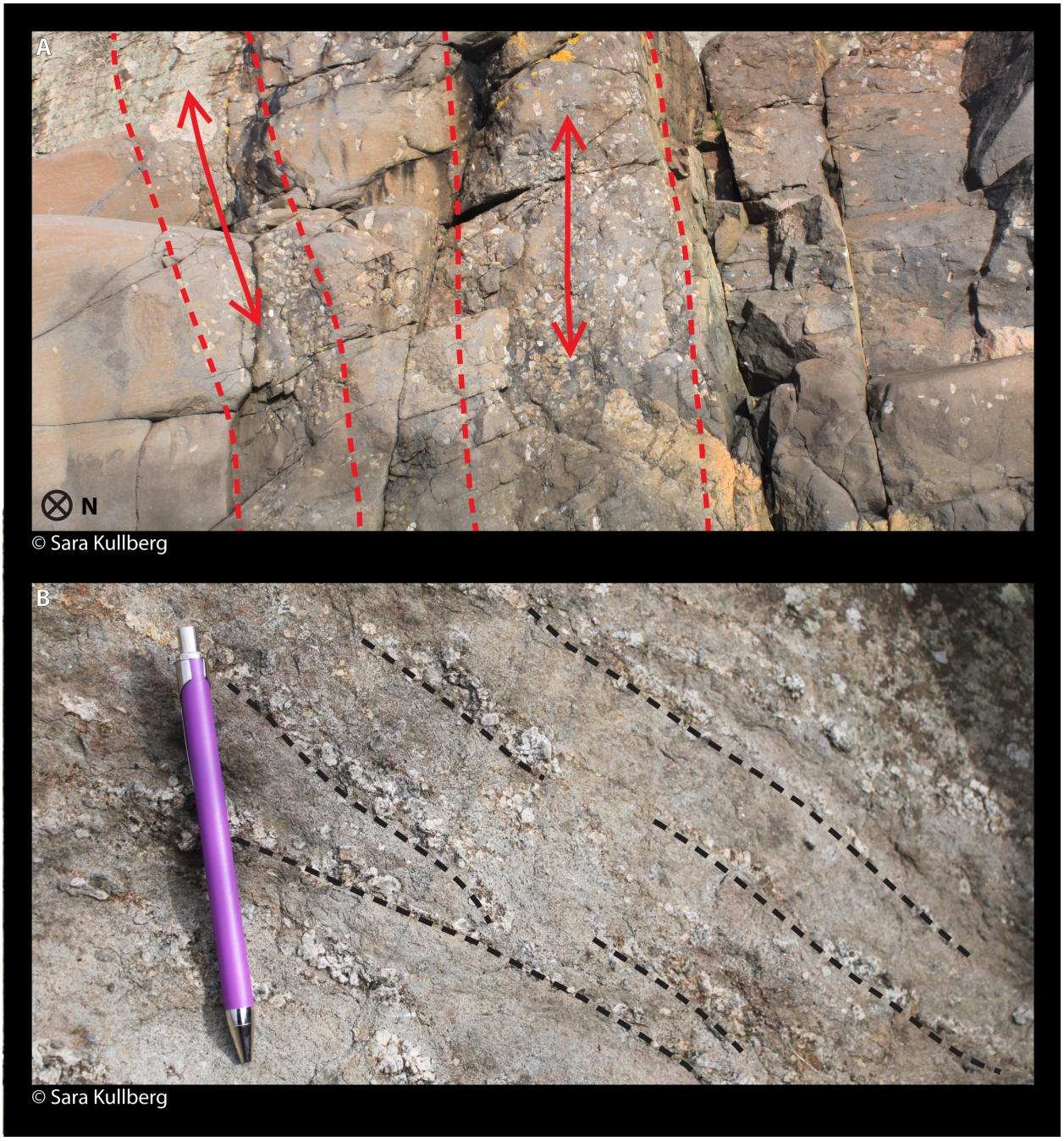

Fig. 24. a) Shows how the plagioclase megacrysts have formed veins. This picture is taken from the outer rim of the norite, a place where magmatic flow structures have not been described earlier. *b)* In the western part of the island anorthosite formed flow-structures within the norite. The general direction is E-W, in accordance with the structures reported within the IRL.

erroneous. Nevertheless, with the petrographic investigation in this study, an abundance of both zircon and baddeleyite have been found, making accurate age determinations possible. It is possible that the zircon, which overprints the primary mineralogy, can give an age of the late magmatic hydration event. Dating baddeleyite, found as inclusions within the ilmenite, would give a relative crystallization sequence of the different lithological units.

Moreover, trace element analysis of ilmenite can give further evidence of crystallization sequence. Further analysis of the relationship between ilmenite and magnetite, as to why some contacts are altered and some are not, could give further insight to mechanisms behind the oxidation as well as an accurate temperature-estimation.

It would also be preferable to do further isotopic studies to elucidate the source region. Although it has been stated that it is difficult to separate a lower mafic crust and upper enriched mantle by simply looking at isotopes (Duchesne *et al*. 1999) several studies regarding Re/Os have proven fruitful (Morgan *et al*. 2000; Schiellerup *et al*. 2000) and could hopefully elucidate the origin for the Hakefjorden Complex as well. Finally, more samples would need to be taken in order to establish a more reliable AFC-model.

9 Conclusions

- All the lithological units belonging to the Hakefjorden Complex crystallized continuously as seen in the gradual change in Mn-content in the ilmenite. The chronological order, from oldest to youngest, is; magnetic vein → oxide aggregate (with or without "snowflakes") → IRL-matrix → anorthosite/norite → norite/altered norite → monzonorite. Anorthosite probably crystallized simultaneously to the magnetic vein, oxide aggregate and the IRL-matrix as well.
- Spider diagrams of incompatible elements show that monzonorite is the most evolved unit, and the magnetic vein, the least evolved. This is in accordance with Mn-results.
- AFC-modelling shows that contamination by the SLM is restricted to the outer monzonorite with an estimated r-value of 0.05.
- Trace element ratios indicate that all the lithological units of the Hakefjorden Complex originate from the same parent.
- The Hakefjorden Complex originates from an enriched source, as made evident by the extreme enrichment of incompatible trace elements. As it is more enriched compared to a metasomatically altered mantle, but displaying low Th-levels it is theorized that the Hakefjorden Complex stems from a lower mafic continental crust.

10 Acknowledgements

A special, and very warm, regard goes to my co-worker Alexandra Glommé for providing me with great support and many brilliant ideas throughout the work. I am also very grateful towards Andreas Petersson for both helping me with practical preparations of the samples as well as proof reading my thesis. Special thanks also go to my supervisor Anders Scherstén for giving me the opportunity to work with this project, and to Victoria Beckman for many inspiring ideas. Warm regards are also given to Martin and Eva Fahlén for providing a lovely work-station during the fieldwork as well as many inspirational talks. Last but not least I would like to thank friends and family for supporting me throughout this process.

11 References

Åhäll, K-I. & Connelly, J.N., 1998: Intermittent 1.53–1.13 magmatism in western Baltica; age constraints and correlations within a postulated supercontinent. *Precambrian Research 92*, 1–20.

Åhäll, K-I. & Connelly, J.N., 2008: Long-term convergence along SW Fennoscandia: 330 m.y. of Proterozoic crustal growth. *Precambriam Research 163*, 402–421.

Åhäll, K-I., Cornell, D.H. & Armstrong, R., 1998: Ion probe zircon dating of three metasedimentary units bordering the Oslo rift: new constraints for early Meso-proterozoic growth of the Baltic Shield. *Precambrian Research 87*, 117–134.

Åhäll, K-I. & Larson, S.Å., 2000: Growt-related 1.85–1.55 Ga magmatism in the Baltic Shield: a review addressing the tectonic characteristics of Svecofennian, TIB 1 - related and Gothian events. *GFF 123*, 59–61.

Årebäck, H., 1995: The Hakefjorden Complex: geology and petrogenesis of a late Sveconorwegian norite-anorthosite intrusion, south-west Sweden. Thesis for Licentiate degree. *Earth sciences centre, Göteborg University A9*.

Årebäck, H., 2001: Petrography, geochemistry and geochronology of mafic to intermediate late Sveconorwegian intrusions: The Hakefjorden Complex and Vinga intrusion, SW Sweden. Doctoral thesis. *Earth sciences centre, Göteborg University A72*.

Årebäck, H. & Andersson, U.B., 2002: Granulite-facies contact metamorphism around the Hakefjorden Norite-Anorthosite Complex, SW Sweden. *Norwegian Journal of Geology 82*, 29–44.

Årebäck, H., Andersson, U.B. & Petersson, J., 2008: Petrological evidence for crustal melting, unmixing, and undercooling in an alkali-calcic, high-level intrusion: the late Sveconorwegian Vinga intrusion, SW Sweden. *Mineralogy and Petrology 91*, 1–46.

Årebäck, H. & Stigh, J., 1997: Polybaric evolution of the Hakefjorden Complex, southwestern Sweden, deduced from partial dissolution in andesine megacrysts. *GFF 119:2*, 97–101.

Årebäck, H. & Stigh, J., 2000: The nature and origin of an anorthosite associated ilmenite-rich leuconorite, Hakefjorden Complex, south-west Sweden. *Lithos 51*, 247–267.

Ashwal, L.D. 1993: *Anorthosites*. Springer Vlg (Berlin/New York) 422 pp.

Bingen, B., Nordgulen, Ø. & Viola, G., 2008: A four-phase model for the Sveconorwegian orogeny, SW Scandinavia. *Norwegian Journal of Geology 88*, 43–72.

Brownlow, A.H., 1996: *Geochemistry* 2nd ed. Prentice Hall. 580 pp.

Buddington, A.F. & Lindsley, D.H., 1964: Iron-titanium oxide minerals and synthetic equivalents. *Journal of Petrology 5(2)*, 310–357.

Charlier, B., Duchesne, J.C. & Vander Auwera, J., 2006: Magma chamber processes in the Tellnes ilmenite deposit (Rogaland anorthosite province, SW Norway) and the formation of Fe-Ti ores in massif-type anorthosites. *Chemical Geology 234*, 264– 290.

Charlier, B., Namur, O., Bolle, O., Latypov, R. & Duchesne, J-C., 2015: Fe-Ti-V-P ore deposits associated with Proterozoic massif-type anorthosites and related rocks. *Earth Science Reviews 141*. 56–81.

Charlier, B., Skår, Ø, Korneliussen, A., Duschesne, J-C. & Auwera, J.V., 2007: Ilmenite composition in the Tellnes Fe-Ti deposit, SW Norway: fractional crystallization, postcumulus evolution and ilmenite -zircon relation. *Contribution to Mineralogy and*

Petrology 154, 119–134.

DePaolo, D.J., 1981: Trace element and isotopic effects of combined wallrock assimilation and fractional crystallization. *Earth and Planetary Science Letters 53*, 189–202.

Duchesne, J.C. & Bingen, B., 2001: The Rogaland anorthosite province: an introduction. *In* Duchesne, J.C. (ed.): The Rogaland intrusive massifs - an excursion guide, 139 pp. *Geological Survey of Norway*.

Duchesne, J.C., Liégeois, J.P., Vander Auwera, J. & Longhi, J., 1999: The crustal tongue melting model and the origin of massive anorthosites. *Terra Nova 11*, 100–105.

Eliasson, T., Ahlin, S. & Petersson, J., 2003: Emplacement mechanism and thermobarometry of the Sveconorwegian Bohus Granite, SW Sweden. *GFF 125*, 113–130.

Eliasson, T. & Schöberg, H., 1991: U-Pb dating of the post-kinematic Sveconorwegian Bohus granite, SW Sweden: evidence of restitic zircon. *Precambrian Research 51*, 337–350.

Fahlén, M., Stigh, J. & Årebäck, H., 2008: Strövtåg på Bohusläns sockertopp. *Grahns tryckeri AB, Lund*, 96 pp.

Frost, R.B., 1991: Introduction to oxygen fugacity and its petrologic importance. *In* P.H. Ribbe (ed.): Oxide minerals: petrologic and magnetic significance 1–9. *Reviews in Mineralogy 25*.

Glommé, A., 2015: $^{87}Sr/^{86}Sr$ in plagioclase, evidence for a crustal origin of the Hakefjorden Complex, SW Sweden. *Dissertations in Geology at Lund University*, No 453, 31 pp. 45 hp (45 ECTS credits).

GeoRoc - Geochemistry of Rocks of the Ocean and Continents 2015-06-02: Convergent margin: http://georoc.mpch-mainz.gwdg.de/georoc/

Gorbatschev, R. & Bogdanova, S., 1993: Frontiers in the Baltic Shield. *Precambrian Research 64*, 3–21.

Haggerty, S.E., 1991: Oxide textures – a mini-atlas. *In* P.H. Ribbe (ed.): Oxide minerals: petrologic and magnetic significance 130–219. *Review in Mineralogy 25*.

Harlov, D., Tropper, P., Seifert, W., Nijland, T. & Förster, H-J., 2006: Formation of Al-rich titanite ($CaTiSiO_4$–$CaAlSiO_4OH$) reaction rims on ilmenite in metamorphic rocks as a function of fH_2O and fO_2. *Lithos 88*, 72–84.

Hellström, F.A., Johansson, Å. & Larson, S.Å., 2004: Age and emplacement of late Sveconorwegian monzogabbroic dykes, SW Sweden. *Precambrian Research 128*, 39–55.

Länsstyrelsen - Västra Götalands län 2015–05–27: http://www.lansstyrelsen.se/vastragotaland/sv/djur–och–natur/skyddad–natur/naturreservat/lanets–naturreservat/kungalv/algon/Pages/index.aspx

Lindsley, D.H., 1991: Experimental studies of oxide minerals. *In* P.H. Ribbe (ed.): Oxide minerals: petrologic and magnetic significance 69–106. *Review in Mineralogy 25*.

Longhi, J., Vander Auwera, J., Fram, M.S. & Duchesne, J-C., 1999: Some phase equilibrium constraints on the origin of Proterozoic (Massif) anorthosites and related rocks. *Journal of Petrology 40*, 339–362.

Morgan, J.W., Stein, H.J., Hannah, J.L., Markey, R.J. & Wiszniewska, J., 2000: Re-Os study of Fe-Ti-V oxide and Fe-Cu-Ni sulphide deposits, Suwałki anorthosite massif, northeast Poland. *Mineralium Deposita 35*, 391–401.

Möller, C., Bingen, B., Andersson, J., Stephens, M.B., Viola, G. & Scherstén, A., 2013: A non-collisional, accretionary Sveconorwegian orogen - comment. *Terra Nova 25(2)*, 165–168.

Petersson, A., Scherstén, A., Bingen, B, Gerdes, A. & Whitehouse, M. J., 2015: Mesoproterozoic continental growth: U-Pb-Hf-O zircon record in the Idefjorden Terrane, Sveconorwegian Orogen. *Precambrian Research 261*, 75–95.

Schärer, U., Wilmart, E. Duchesne, J.C., 1996: The short duration and anorogenic character of anorthosite magmatism: U-Pb dating of the Rogaland complex, Norway. *Earth and Planetary Science Letters 139*, 335–350.

Scherstén, A., Årebäck, H., Cornell, D., Hoskin, P., Åberg, A. & Armstrong, R., 2000: Dating mafic-ultramafic intrusions by ion-microprobing contact-melt zircon: examples from SW Sweden. *Contributions to Mineralogy and Petrology 139*, 115–125.

Schiellerup, H., Lambert, D.D., Prestvik, T., Robins, B., McBride, J.S. & Larsen, R.B., 2000: Re-Os isotopic evidence for a lower crustal origin of massif-type anorthosites. *Nature 405*, 781–784.

Simmons, E.C., & Hanson, G.N., 1978: Geochemistry and Origin of Massif-Type Anorthosites. *Contributions to Mineralogy and Petrology 66*, 119–135.

Slagstad, T., Roberts, N.M.W., Marker, M., Røhr, T.S. & Schiellerup, H., 2013: A non-collisional, accretionary Sveconorwegian orogen. *Terra Nova 25*, 30–37.

Söderlund, U., Möller, C., Andersson, J., Johansson, L. & Whitehouse, M., 2002: Zircon geochronology in polymetamorphic gneisses in the Sveconorwegian orogeny, SW Sweden: ion microprobe evidence for 1.46–1.42 and 0.98–0.96 Ga reworking. *Precambrian Research 113*, 193–225.

Toplis, M.J., Libourel, G. & Carroll, M.R., 1994: The role of phosphorus in crystallization processes of basalt: An experimental study. *Geochimica et Cosmochimica 58*, 797–810.

Vander Auwera, J. & Longhi, J., 1994: Experimental study of a jotunite (hyperstene monzodiorite): constraints on the parent magma composition and crystallization conditions (P, T, fO_2) of the Bjerkreim-Sokndal layered intrusion (Norway). *Contributions to Mineralogy and Petrology 118*, 60–78.

Vidal, Ph., Dupuy, C., Maury, R. & Richard, M., 1989: Mantle metasomatism above subduction zones: trace element and radiogenic isotope charac-

teristics of peridotite xenoliths from Batan Island (Philippines). *Geology 17*, 1115–1118.

Winter, J.D., 2009: *Principles of igneous and metamorphic petrology 2nd ed*. Pearson Prentice Hall (USA), 702 pp.

Wyatt, B.A., 1977: The melting and crystallisation behaviour of a natural clinopyroxene-ilmenite intergrowth. *Contributions to Mineralogy and Petrology 61*, 1–9.

AFC	Assimilation Fractional Crystallization
Amph	Amphibole
Badd	Baddeleyite
Cpx	Clinopyroxene
$FeTiO_3$	Ilmenite
Fe_2O_3	Hematite
Fe_2SiO_4	Fayalite
Fe_2TiO_4	Ulvöspinel
Fe_3O_4	Magnetite
Hem	Hematite
HFC	Hakefjorden Complex
Ilm	Ilmenite
IRL	Ilmenite-Rich Leuconorite
Mt	Magnetite
Qz	Quartz
Rt	Rutile
SiO_2	Quartz
SLM	Stora Le-Marstrand
”Snowflakes”	Poikilitic plagioclase with a snowflake-like appearance
Tit	Titanite
Tit-aug	Titan-augite
Tit-hem	Titano-hematite
Usp	Ulvöspinel
Zr	Zircon

Sample nr	Rock description	North	East
AGSE03	Norite with plagioclase megacryst	57°55.365	011°40.787
AGSE04	Norite with plagioclase megacryst	57°55.365	011°40.787
AGSE05	Quartz-vein in norite	57°55.365	011°40.787
AGSE06	Plagioclase megacryst	57°55.365	011°40.787
AGSE07	Anorthosite	57°55.502	011°40.916
AGSKSE03(1)	IRL-matrix	57°55.434	011°41.095
AGSKSE03(2)	IRL-matrix	57°55.434	011°41.095
AGSKSE03(3)	IRL-matrix	57°55.434	011°41.095
AGSKSE04	Altered norite	57°55.491	011°41.119
AGSKSE06	Altered norite	57°55.431	011°41.121
AGSKSE08	IRL-matrix	57°55.431	011°41.121
AGSKSE09(1)	Altered norite	57°55.430	011°41.107
AGSKSE09(2)	Altered norite	57°55.430	011°41.107
AGSKSE10	Norite	57°55.431	011°41.121
AGSKSE11	Magnetic vein	57°55.431	011°41.121
AGSKSE17	Oxide aggregate	57°55.455	011°41.125
AGSKSE21(1)	Mafic enclave	57°55.369	011°40.703
AGSKSE21(2)	Mafic enclave	57°55.369	011°40.703
AGSKSE22(1)	Altered norite	57°55.369	011°40.736
AGSKSE22(2)	Altered norite	57°55.369	011°40.736
AGSKSE23	Altered norite	57°55.460	011°41.187
AGSKSE24	SLM	57°55.233	011°41.880
AGSKSE25	Monzonorite	57°55.363	011°41.388

Lithogeochemistry

ICP / ICP MS (LF100- CDN$ 29.40, LF200-CDN$48.05, LF202 - CDN$58.80, LF300 - CDN$25.60)

		ELEMENT	DETECTION LIMIT	UPPER LIMIT
LF200	LF300	SiO_2	0.01 %	100 %
		Al_2O_3	0.01 %	100 %
		CaO	0.01 %	100 %
		Cr_2O_3	0.002 %	100 %
		Fe_2O_3	0.04 %	100 %
		K_2O	0.01 %	100 %
		MgO	0.01 %	100 %
		MnO	0.01 %	100 %
		Na_2O	0.01 %	100 %
		P_2O_5	0.01 %	100 %
		TiO_2	0.01 %	100 %
		Ba	5 ppm	5 %
		Nb	5 ppm	50,000 ppm
		Ni	20 ppm	10,000 ppm
		Sc	1 ppm	10,000 ppm
		Sr	2 ppm	50,000 ppm
		Y	3 ppm	50,000 ppm
		Zn	5 ppm	50,000 ppm
		LOI	0.1 %	100 %
		Sum	0.01 %	100 %
	LF300EXT	Ce	30 ppm	50 000 ppm
		Co	20 ppm	10 000 ppm
		Cu	5 ppm	10 000 ppm
		Zn	5 ppm	10 000 ppm
	LF100	Ba	1 ppm	50,000 ppm
		Be	1 ppm	10,000 ppm
		Ce	0.1 ppm	50,000 ppm
		Co	0.2 ppm	10,000 ppm
		Cs	0.1 ppm	10,000 ppm
		Dy	0.05 ppm	10,000 ppm
		Er	0.03 ppm	10,000 ppm
		Eu	0.02 ppm	10,000 ppm
		Ga	0.5 ppm	10,000 ppm
		Gd	0.05 ppm	10,000 ppm
		Hf	0.1 ppm	10,000 ppm
		Ho	0.02 ppm	10,000 ppm
		La	0.1 ppm	50,000 ppm
		Lu	0.01 ppm	10,000 ppm
		Nb	0.1 ppm	50,000 ppm
		Nd	0.3 ppm	10,000 ppm
		Pr	0.02 ppm	10,000 ppm
		Rb	0.1 ppm	10,000 ppm
		Sm	0.05 ppm	10,000 ppm
		Sn	1 ppm	10,000 ppm
		Sr	0.5 ppm	50,000 ppm
		Ta	0.1 ppm	50,000 ppm
		Tb	0.01 ppm	10,000 ppm
		Th	0.2 ppm	10,000 ppm
		Tm	0.01 ppm	10,000 ppm
		U	0.1 ppm	10,000 ppm

		ELEMENT	DETECTION LIMIT	UPPER LIMIT
LF200	LF100	V	8 ppm	10,000 ppm
		W	0.5 ppm	10,000 ppm
		Y	0.1 ppm	50,000 ppm
		Yb	0.05 ppm	10,000 ppm
		Zr	0.1 ppm	50,000 ppm

Add on Elements from AQ200

	ELEMENT	DETECTION LIMIT	UPPER LIMIT
LF202	Ag	0.1 ppm	100 ppm
	As	0.5 ppm	10,000 ppm
	Au	0.5 ppb	100,000 ppb
	Bi	0.1 ppm	2,000 ppm
	Cd	0.1 ppm	2,000 ppm
	Cu	0.1 ppm	10,000 ppm
	Hg	0.01 ppm	50 ppm
	Mo	0.1 ppm	2,000 ppm
	Ni	0.1 ppm	10,000 ppm
	Pb	0.1 ppm	10,000 ppm
	Sb	0.1 ppm	2,000 ppm
	Se	0.5 ppm	100 ppm
	Tl	0.1 ppm	1,000 ppm
	Zn	1 ppm	10,000 ppm

Leco from TC000

	ELEMENT	DETECTION LIMIT	UPPER LIMIT
LF202	C	0.02 %	100 %
	S	0.02 %	100 %

	Altered norite				*Mafic enclave*	*IRL-matrix*		*Magnetic vein*	*Oxide aggregate*	*Norite*	*Monzo-norite*	*SLM*	*Anorthosite*	*IRL-matrix*
	AGSKSE04	**AGSKSE09**	**AGSKSE22**	**AGSKSE23**	**AGSKSE21**	**AGSKSE08**	**AGSKSE03-1**	**AGSKSE11**	**AGSKSE03-2**	**AGSKSE10**	**AGSKSE25**	**AGSKSE24**	**AGSE07**	**B7b**
SiO_2	49.7	53.0	52.9	52.2	51.2	18.6	26.2	10.8	11.6	52.3	64.1	78.1	56.7	20.7
TiO_2	1.4	2.9	1.9	2.7	4.1	29.0	22.8	35.8	35.0	2.5	1.4	0.5	0.2	28.3
Al_2O_3	23.1	20.4	19.8	17.2	14.4	8.7	11.8	5.1	5.2	17.4	14.6	11.2	26.3	8.8
FeO	6.1	6.9	7.3	9.6	12.7	34.0	28.0	41.2	40.2	9.5	6.7	2.5	1.0	33.1
MnO	0.1	0.1	0.1	0.1	0.2	0.2	0.2	0.2	0.2	0.1	0.1	0.0	0.0	0.2
MgO	3.0	2.3	4.3	5.7	3.7	4.0	3.4	3.9	4.3	6.1	1.4	0.7	0.3	3.7
CaO	11.6	7.8	8.3	7.2	7.0	3.3	4.5	1.7	1.9	7.3	3.3	0.5	8.6	3.2
Na_2O	3.6	4.3	3.7	3.1	3.6	1.4	2.0	0.6	0.8	3.1	3.6	1.7	5.9	1.2
K_2O	1.3	1.7	1.3	1.6	2.0	0.3	0.6	0.2	0.2	1.1	4.4	4.5	0.8	0.2
P_2O_5	0.1	0.6	0.4	0.6	1.2	0.1	0.2	0.1	0.1	0.6	0.4	0.1	0.0	0.2
Cr_2O_3	0.0	0.0	0.0	0.0	0.0	0.4	0.3	0.5	0.5	0.0	0.0	0.0	0.0	0.4
Sum	100.0	100.0	100.0	100.0	100.0	100.0	100.0	100.0	100.0	100.0	100.0	100.0	100.0	100.0
Sc	17.0	11.0	12.0	16.0	20.0	41.0	34.0	47.0	47.0	16.0	14.0	7.0	<1	40.8
Ti	7853.6	16726.3	10971.0	15707.2	23980.4	169121.8	132851.4	206351.3	202934.1	14208.4	8453.1	3117.5	1438.8	163666.2
V	205.0	144.0	111.0	148.0	213.0	1178.0	989.0	1417.0	1404.0	150.0	51.0	41.0	14.0	
Cr	102.6	102.6	191.6	164.2	47.9	2470.0	2162.1	3359.4	3544.2	266.8		20.5		3300.0
Co	41.9	41.5	50.3	54.4	67.4	55.5	60.4	86.8	88.2	65.8	57.1	88.6	35.2	120.0
Ni	35.4	39.0	23.3	71.3	26.7	47.9	42.6	174.6	33.3	66.8	1.9	5.6	3.3	
Cu	12.9	61.5	18.7	51.4	23.2	25.6	22.0	40.1	20.1	40.6	8.5	6.9	4.4	
Zn	24.0	50.0	30.0	41.0	79.0	8.0	9.0	11.0	10.0	73.0	77.0	41.0	5.0	180.0
Ga	19.7	23.4	24.4	22.2	26.3	16.8	19.4	14.2	15.8	19.0	25.3	11.1	15.7	
Rb	36.9	37.1	28.5	41.7	49.0	4.1	10.2	2.8	5.3	31.0	85.0	134.7	6.6	19.0
Sr	736.2	727.9	672.4	602.5	547.0	307.8	424.6	157.1	172.7	561.5	315.8	132.8	997.9	184.0
Y	9.3	32.4	24.5	34.1	61.2	6.3	10.3	5.2	6.5	28.9	80.9	28.2	1.8	
Zr	61.0	219.1	203.7	278.0	545.9	306.4	289.0	360.6	365.9	251.2	955.9	325.6	9.8	179.0
Nb	2.6	9.5	10.2	13.5	27.7	32.9	28.4	36.7	38.2	11.9	30.8	13.0	0.4	38.0
Cs	4.7	1.8	0.7	4.1	0.4	0.1	<0.1	0.3	<0.1	2.4	2.7	8.1	<0.1	2.0
Ba	264.0	668.0	479.0	576.0	952.0	175.0	272.0	79.0	128.0	346.0	1387.0	893.0	210.0	144.0
La	9.2	41.1	26.1	39.0	72.6	7.7	14.0	4.7	8.0	34.5	78.0	39.3	2.7	10.3
Ce	18.9	92.0	56.2	85.3	161.6	15.9	29.5	9.8	16.8	74.9	183.7	81.9	4.7	22.0
Pr	2.5	11.6	7.2	11.3	20.7	1.9	3.9	1.3	2.2	9.9	24.0	9.7	0.6	
Nd	12.0	47.8	30.7	47.6	85.9	8.4	15.1	5.3	9.2	42.2	101.3	36.0	2.5	10.0
Sm	2.5	9.4	6.4	9.4	17.2	1.6	3.0	1.1	1.7	8.1	20.0	6.3	0.5	2.1
Eu	1.0	2.5	2.0	2.5	4.5	0.7	1.1	0.4	0.6	2.4	4.5	1.1	0.7	1.0
Gd	2.5	8.6	6.2	8.4	16.2	1.4	2.9	1.0	1.7	7.3	18.6	5.4	0.5	
Tb	0.4	1.3	0.9	1.2	2.3	0.2	0.4	0.2	0.2	1.1	3.0	0.9	0.1	
Dy	2.0	6.6	5.2	7.0	12.4	1.2	2.3	1.0	1.4	6.0	16.6	5.4	0.3	
Ho	0.4	1.1	0.9	1.2	2.2	0.2	0.4	0.2	0.3	1.0	3.1	1.0	0.1	
Er	1.1	3.1	2.3	3.4	5.9	0.7	1.1	0.6	0.8	2.8	8.5	3.1	0.1	
Tm	0.1	0.4	0.3	0.5	0.8	0.1	0.2	0.1	0.1	0.4	1.3	0.5	0.0	
Yb	0.9	2.5	2.1	2.9	5.2	0.8	1.1	0.8	0.9	2.5	7.7	3.3	0.1	1.0
Reference	1	1	1	1	1	1	1	1	1	1	1	1	1	2

	Altered norite				*Mafic enclave*	*IRL-matrix*		*Magnetic vein*	*Oxide aggregate*	*Norite*	*Monzo-norite*	*SLM*	*Anorthosite*	*IRL-matrix*
	AGSKSE04	**AGSKSE09**	**AGSKSE22**	**AGSKSE23**	**AGSKSE21**	**AGSKSE08**	**AGSKSE03-1**	**AGSKSE11**	**AGSKSE03-2**	**AGSKSE10**	**AGSKSE25**	**AGSKSE24**	**AGSE07**	**B7b**
Lu	0.1	0.4	0.3	0.4	0.7	0.1	0.2	0.1	0.1	0.4	1.2	0.6	0.0	0.2
Hf	0.3	6.3	6.7	9.1	4.7	5.7	9.5	7.7	1.6	9.9	8.5	22.8	9.4	8.3
Ta	2.0	2.6	1.0	1.7	0.8	0.7	0.2	2.9	<0.1	2.0	0.7	2.1		1.0
Pb	1.3	3.9	1.5	2.3	1.4	1.4	1.3	2.0	1.4	1.9	13.8	8.6	0.4	
Th	0.6	3.9	2.0	3.6	4.9	0.5	1.1	0.3	0.6	3.2	5.8	14.5	<0.2	
U	0.2	0.9	0.6	0.8	1.2	0.2	0.3	<0.1	0.2	0.8	3.0	3.9	<0.1	0.5
Au	0.0	0.0	0.0	0.0	0.0	0.0	0.0	0.0	0.0	0.0	0.0	0.0	0.0	
TiO_2/Zr														
Ti/V	38.3	116.2	98.8	106.1	112.6	143.6	134.3	145.6	144.5	94.7	165.7	76.0	102.8	
La/U	46.0	45.7	43.5	48.8	60.5	38.5	46.7		40.0	43.1	26.0	10.1		20.6
Nb/La	0.3	0.2	0.4	0.3	0.4	4.3	2.0	7.8	4.8	0.3	0.4	0.3	0.1	3.7
Nb/Ba	0.0	0.0	0.0	0.0	0.0	0.2	0.1	0.5	0.3	0.0	0.0	0.0	0.0	0.3
Nb/U	13.0	10.6	17.0	16.9	23.1	164.5	94.7		191.0	14.9	10.3	3.3		76.0
Nb/Zr	0.0	0.0	0.1	0.0	0.1	0.1	0.1	0.1	0.1	0.0	0.0	0.0	0.0	0.2
Nb/Hf	8.7	1.5	1.5	1.5	5.9	5.8	3.0	4.8	23.9	1.2	3.6	0.6	0.0	4.6
Nb/Y	0.3	0.3	0.4	0.4	0.5	5.2	2.8	7.1	5.9	0.4	0.4	0.5	0.2	
Th-1	1.7	0.3	0.5	0.3	0.2	2.0	0.9	3.3	1.7	0.3	0.2	0.1		
Nb/Th	4.3	2.4	5.1	3.8	5.7	65.8	25.8	122.3	63.7	3.7	5.3	0.9		
Ce/Pb	14.5	23.6	37.5	37.1	115.4	11.4	22.7	4.9	12.0	39.4	13.3	9.5	11.8	
Nb/Nb*	0.5	0.3	0.6	0.5	0.6	6.8	2.9	12.6	7.1	0.5	0.6	0.2		
Ti/Ti*	0.5	0.4	0.3	0.3	0.3	16.5	7.2	28.4	19.8	0.3	0.1	0.1	0.3	
Zr/Zr*	188.2	174.6	244.8	221.8	240.0	1412.2	729.2	2582.8	1572.6	229.0	358.6	364.4	156.1	660.0
La/SmN	2.3	2.7	2.5	2.6	2.7	3.0	3.0	2.8	3.0	2.7	2.4	3.9	3.8	3.1
Gd/YbN	2.4	2.8	2.4	2.4	2.5	1.4	2.2	1.1	1.5	2.4	1.9	1.3	3.6	0.0
La/YbN	7.3	11.1	8.5	9.1	9.5	6.7	8.7	4.2	6.1	9.4	6.8	8.1	18.2	6.9
Eu/Eu*	1.2	0.8	1.0	0.9	0.8	1.4	1.2	1.2	1.0	0.9	0.7	0.6	4.7	
Sr/Nd	61.4	15.2	21.9	12.7	6.4	36.6	28.1	29.6	18.8	13.3	3.1	3.7	399.2	18.4
LaN	29.7	132.6	84.2	125.8	234.2	24.8	45.2	15.2	25.8	111.3	251.6	126.8	8.7	33.2
CeN	23.4	113.9	69.6	105.6	200.0	19.7	36.5	12.1	20.8	92.7	227.4	101.4	5.8	27.2
PrN	20.8	95.3	59.1	92.4	169.3	15.7	31.9	10.5	17.6	81.2	196.3	79.5	4.8	
NdN	20.0	79.7	51.2	79.3	143.2	14.0	25.2	8.8	15.3	70.3	168.8	60.0	4.2	16.7
SmN	12.8	48.2	33.0	48.3	88.2	8.2	15.2	5.4	8.6	41.7	102.7	32.5	2.3	10.8
EuN	13.6	33.7	27.8	34.0	60.8	9.5	15.4	5.6	7.8	32.2	61.4	14.6	9.4	13.6
GdN	9.7	33.0	23.7	32.5	62.7	5.3	11.2	3.9	6.5	28.3	71.7	20.8	1.7	
TbN	8.2	26.6	19.6	26.2	49.4	4.4	8.4	3.4	5.1	22.8	62.9	19.0	1.3	
DyN	6.2	20.6	16.1	21.7	38.5	3.6	7.2	3.1	4.4	18.6	51.6	16.8	1.0	
HoN	5.6	15.6	12.1	16.6	30.5	2.9	6.0	2.8	3.5	14.5	42.6	14.5	0.7	
ErN	5.2	14.6	11.0	16.0	28.1	3.3	5.3	3.0	3.8	13.5	40.2	14.9	0.7	
TmN	4.3	13.6	10.5	14.5	25.3	3.1	4.9	2.8	3.4	13.0	39.2	15.4	0.6	
YbN	4.1	12.0	10.0	13.8	24.6	3.7	5.2	3.6	4.2	11.9	37.0	15.6	0.5	4.8
LuN	3.7	11.5	9.6	13.4	23.0	4.3	5.6	4.0	4.3	12.4	37.0	17.1	0.6	4.7
Reference	1	1	1	1	1	1	1	1	1	1	1	1	1	2

	IRL-matrix **93081b**	*IRL-matrix* **97008**	*IRL-matrix* **98003**	*Norite* **A18b**	*Norite* **B14b**	*Norite* **C5b**	*Norite* **B6b**	*PM* **PM**	*Upper CC* **Upper CC**	*Middle CC* **Middle CC**	*Lower CC* **Lower CC**	*Average CC* **Average CC**	*N-MORB* **N-MORB**
SiO_2	15.1	35.9	31.8	51.9	45.8	50.1	51.9	45.8	66.6	63.5	53.4	60.5	51.3
TiO_2	32.8	15.7	18.1	3.1	5.6	3.5	2.3	0.2	0.6	0.7	0.8	0.7	1.6
Al_2O_3	6.6	15.8	14.5	15.9	12.3	13.9	17.5	4.5	15.4	15.0	16.9	15.9	15.5
FeO	37.1	19.9	23.1	11.6	16.7	13.3	9.8	8.2	5.0	6.0	8.6	6.7	9.5
MnO	0.2	0.1	0.2	0.2	0.2	0.2	0.1	0.1	0.1	0.1	0.1	0.1	0.1
MgO	3.7	3.1	3.7	4.8	6.3	4.1	6.6	37.1	2.5	3.6	7.2	4.7	7.7
CaO	2.2	5.9	5.4	7.1	7.2	8.3	7.6	3.7	3.6	5.3	9.6	6.4	11.5
Na_2O	0.9	2.5	2.2	3.0	2.2	2.7	2.9	0.4	3.3	3.4	2.7	3.1	2.6
K_2O	0.2	0.7	0.6	1.7	1.3	2.0	0.9	0.0	2.8	2.3	0.6	1.8	0.1
P_2O_5	0.1	0.4	0.3	0.7	1.8	1.9	0.3	0.0	0.1	0.2	0.1	0.1	0.0
Cr_2O_3	1.0	0.0	0.0	0.1	0.4	0.0	0.1	0.0	0.0	0.0	0.0	0.0	0.0
Sum	100.0	100.0	100.0	100.0	100.0	100.0	100.0	100.0	100.0	100.0	100.0	100.0	100.0
Sc	41.4	26.0	30.0	16.6	19.6	20.3	14.0	16.5	14.0	19.0	31.0	21.9	41.4
Ti	191243.7	92324.5	106712.8	17985.3	32793.2	20443.3	13369.1	1280.0	3813.1	4109.8	4871.0	4280.2	9741.2
V	1220.0	631.0	739.0					86.0	97.0	107.0	196.0	138.0	
Cr	1940.0	1000.0	1300.0	710.0	11.0	6.0	460.0	2520.0	92.0	76.0	215.0	135.0	
Co		32.0	45.0	60.0	110.0	55.0	66.0	102.0	17.3	22.0	38.0	26.6	47.1
Ni	103.0	129.0	172.0					1860.0	47.0	33.5	88.0	59.0	149.5
Cu	39.5	30.1	114.0					20.0	28.0	26.0	26.0	27.0	74.4
Zn	177.0	111.0	122.0	100.0	160.0	140.0	90.0	53.5	67.0	69.5	78.0	72.0	
Ga								4.4	17.5	17.5	13.0	16.0	
Rb	14.0			43.0	11.0	38.0	21.0	0.6	82.0	65.0	11.0	49.0	1.3
Sr	134.0	566.0	525.0	451.0	347.0	423.0	547.0	20.3	320.0	282.0	348.0	320.0	113.2
Y	18.0	17.0	12.0	18.0	44.0	55.0	23.0	4.4	21.0	20.0	16.0	19.0	35.8
Zr	212.0	213.0	216.0	330.0	291.0	363.0	150.0	10.8	193.0	149.0	68.0	132.0	104.2
Nb	30.0	30.0	34.0	25.0	38.0	28.0	19.0	0.6	12.0	10.0	5.0	8.0	3.5
Cs		1.0		2.0	2.0		1.0	0.0	4.9	2.2	0.3	2.0	0.0
Ba	142.0	314.0	289.0	525.0	336.0	563.0	252.0	6.8	628.0	532.0	259.0	456.0	13.9
La	42.0	21.5	15.1	36.6	41.8	58.4	18.1	0.7	31.0	24.0	8.0	20.0	3.9
Ce	13.0	47.0	32.0	78.0	90.0	126.0	40.0	1.8	63.0	53.0	20.0	43.0	12.0
Pr								0.3	7.1	5.8	2.4	4.9	2.1
Nd	6.0	24.0	15.0	40.0	47.0	68.0	20.0	1.3	27.0	25.0	11.0	20.0	11.2
Sm	1.2	4.7	3.2	9.1	10.7	15.3	4.3	0.4	4.7	4.6	2.8	3.9	3.8
Eu	0.5	1.7	0.9	2.7	2.6	3.5	1.6	0.2	1.0	1.4	1.1	1.1	1.3
Gd								0.6	4.0	4.0	3.1	3.7	5.1
Tb		0.6		1.3	1.5	2.2	0.5	0.1	0.7	0.7	0.5	0.6	0.9
Dy								0.7	3.9	3.8	3.1	3.6	6.3
Ho								0.2	0.8	0.8	0.7	0.8	1.3
Er								0.5	2.3	2.3	1.9	2.1	4.1
Tm								0.1	0.3	0.3	0.2	0.3	0.6
Yb	0.8	1.5	1.1	3.0	3.0	4.3	1.4	0.5	2.0	2.2	1.5	1.9	3.9
Reference	2	2	2	2	2	2	2	3	4	4	4	4	5

	IRL-matrix	*IRL-matrix*	*IRL-matrix*	*Norite*	*Norite*	*Norite*	*Norite*	*PM*	*Upper CC*	*Middle CC*	*Lower CC*	*Average CC*	*N-MORB*
	93081b	**97008.0**	**98003.0**	**A18b**	**B14b**	**C5b**	**B6b**	**PM**	**Upper CC**	**Middle CC**	**Lower CC**	**Average CC**	**N-MORB**
Lu	0.1	0.2	0.2	0.5	0.4	0.6	0.2	0.1	0.3	0.4	0.3	0.3	0.6
Hf	7.0	7.0	9.1	0.5	9.6	4.1		0.3	5.3	4.4	1.9	3.7	3.0
Ta	1.0		1.0	1.0	1.0			0.0	0.9	0.6	0.6	0.7	0.2
Pb								0.2	17.0	15.2	4.0	11.0	0.5
Th		1.0	1.0	2.3	2.3	4.2	1.2	0.1	10.5	6.5	1.2	5.6	0.2
U		0.5		0.6	0.9	1.1		0.0	2.7	1.3	0.2	1.3	0.1
Au													
TiO_2/Zr								0.0	0.0	0.0	0.0	0.0	0.0
Ti/V	156.8	146.3	144.4					14.9	39.3	38.4	24.9	31.0	
La/U		43.0		61.0	46.4	53.1		31.5	11.5	18.5	40.0	15.4	54.8
Nb/La	0.7	1.4	2.3	0.7	0.9	0.5	1.0	0.9	0.4	0.4	0.6	0.4	0.9
Nb/Ba	0.2	0.1	0.1	0.0	0.1	0.0	0.1	0.1	0.0	0.0	0.0	0.0	0.3
Nb/U		60.0		41.7	42.2	25.5		27.0	4.4	7.7	25.0	6.2	49.3
Nb/Zr	0.1	0.1	0.2	0.1	0.1	0.1	0.1	0.1	0.1	0.1	0.1	0.1	0.0
Nb/Hf	4.3	4.3	3.7	50.0	4.0	6.8		2.0	2.3	2.3	2.6	2.2	1.2
Nb/Y	1.7	1.8	2.8	1.4	0.9	0.5	0.8	0.1	0.6	0.5	0.3	0.4	0.1
Th-1		1.0	1.0	0.4	0.4	0.2	0.8	12.0	0.1	0.2	0.8	0.2	5.3
Nb/Th		30.0	34.0	10.9	16.5	6.7	15.8	7.1	1.1	1.5	4.2	1.4	18.7
Ce/Pb								9.7	3.7	3.5	5.0	3.9	24.5
Nb/Nb*		2.6	3.6	1.1	1.6	0.7	1.7	1.0	0.3	0.3	0.7	0.3	1.7
Ti/Ti*								1.0	0.5	0.5	0.7	0.6	0.9
Zr/Zr*	1335.0	338.9	526.8	292.3	219.3	190.2	273.3	1.0	1.2	1.0	0.9	1.0	1.1
La/SmN	22.0	2.9	3.0	2.5	2.5	2.4	2.6	1.0	4.1	3.3	1.8	3.2	0.7
Gd/YbN	0.0	0.0	0.0	0.0	0.0	0.0	0.0	1.0	1.6	1.5	1.7	1.6	1.1
La/YbN	35.4	9.7	9.2	8.2	9.4	9.1	8.7	1.0	10.4	7.3	3.6	7.1	0.7
Eu/Eu*								1.0	0.7	1.0	1.1	0.9	0.9
Sr/Nd	22.3	23.6	35.0	11.3	7.4	6.2	27.4	15.3	11.9	11.3	31.6	16.0	10.1
LaN	135.5	69.4	48.7	118.1	134.8	188.4	58.4	2.2	100.0	77.4	25.8	64.5	12.6
CeN	16.1	58.2	39.6	96.5	111.4	155.9	49.5	2.2	78.0	65.6	24.8	53.2	14.9
PrN								2.2	58.2	47.5	19.7	40.2	17.0
NdN	10.0	40.0	25.0	66.7	78.3	113.3	33.3	2.2	45.0	41.7	18.3	33.3	18.6
SmN	6.2	24.1	16.4	46.7	54.9	78.5	22.1	2.2	24.1	23.6	14.4	20.0	19.2
EuN	6.8	23.1	12.2	36.7	35.4	47.6	21.8	2.2	13.6	19.0	15.0	15.0	18.2
GdN								2.2	15.4	15.4	12.0	14.3	19.6
TbN		12.7	0.0	27.4	31.6	46.4	10.5	2.2	14.8	14.8	10.1	12.7	18.7
DyN								2.2	12.1	11.8	9.6	11.2	19.6
HoN								2.2	11.6	11.4	9.5	10.7	18.7
ErN								2.2	11.0	11.0	9.0	10.0	19.7
TmN								2.2	9.3	9.9	7.4	8.6	19.2
YbN	3.8	7.2	5.3	14.4	14.4	20.6	6.7	2.2	9.6	10.5	7.2	9.1	18.7
LuN	3.7	6.2	5.6	14.0	13.4	18.3	6.2	2.2	9.6	12.4	7.8	9.3	18.3
Reference	2	2	2	2	2	2	2	3	4	4	4	4	5

References	
1	This thesis
2	Årebäck 1995
3	Palme & O'Neill 2003
4	Rudnick & Gao 2003
5	Hoffman 1988

	Opx	Ref.	Cpx	Ref.	Ilm	Ref.	Mt	Ref.	Plag	Ref.	Ap	Ref.
K			*0.0072*	2					*0.3*	10		
Rb												
Sr	*0.0012*	1	*0.157*	3					*2*	6		
Cs			*0.0058*	3								
Ba			*0.0058*	3					*0.68*	7		
Pb^{2+}			*0.0102*	3					*0.36*	6		
Ti			*0.451*	3	*>100*		*>1*		*0.04*	6		
V			*1.81*	3								
Zr	*0.032*	1	*0.195*	3	*0.28*	5						
Nb	*0.0013*	1	*0.0081*	3	*0.8*	5			*0.01*	6		
Hf	*0.06*	1	*0.223*	3					*0.01*	6		
Ta	*0.0025*	1										
Th			*0.014*	3					*0.05*	6		
U	*0.0001*	9	*0.0127*	3	*0.008*	8			*0.11*	6		
Sc			*0.808*	3	*1.8*	7	*0.73*	4	*0.08*	7	*0.22*	7
Y	*0.095*	1	*0.467*	2								
La	*0.0008*	1	*0.0515*	3	*0.098*	7	*0.015*	4	*0.27*	6	*8.6*	7
Ce	*0.0016*	1	*0.108*	3	*0.11*	7	*0.016*	4	*0.2*	6	*11.2*	7
Pr	*0.0032*	1	*0.15*	6					*0.17*	6		
Nd	*0.0056*	1	*0.277*	3	*0.14*	7	*0.026*	4	*0.14*	6	*14*	7
Sm	*0.015*	1	*0.462*	3	*0.15*	7	*0.024*	4	*0.11*	6	*14.6*	7
Eu	*0.03*	1	*0.458*	3	*0.1*	7	*0.025*	4	*0.73*	6	*9.6*	7
Gd	*0.034*	1	*0.3*	6	*0.14*	7	*0.018*	4	*0.066*	6	*15.8*	7
Tb	*0.054*	1	*0.31*	6	*0.14*	7	*0.018*	4	*0.06*	6	*15.4*	7
Dy	*0.077*	1	*0.711*	3					*0.055*	6		
Ho	*0.1*	1	*0.44*	3	*0.13*	7	*0.017*	4	*0.048*	6	*13.3*	7
Er	*0.12*	1	*0.66*	3					*0.041*	6		
Tm									*0.036*	6		
Yb	*0.22*	1	*0.633*	3	*0.17*	7	*0.018*	4	*0.031*	6	*8.1*	7
Lu	*0.22*	1	*0.623*	3					*0.025*	6		
Cr			*1.66*	3								
Co					*2.2*	7	*3.4*	4	*0.026*	7		
Ni												
Cu					*1.46*	7	*0.42*	4	*0.004*	7	*0.28*	7
Zn					*0.38*	7	*2.6*	4	*0.13*	7		
Ga					*0.14*	7	*2*	4	*1.7*	7		

1 = Green *et al* . 2000
2 = Hart & Dunn 1993
3 = Hauri *et al* . 1994
4 = Lemarchand *et al* . 1987
5 = McCallum & Charette 1978
6 = McKenzie & O'Nions 1991
7 = Paster *et al* . 1974
8 = Zack & Brumm 1998
9 = Klemme *et al* . 2006
10 = Aignertorres *et al* . 2007

Opx = Orthopyroxene
Cpx = Clinopyroxene
Ilm = Ilmenite
Mt = Magnetite
Plag = Plagioclase
Ap = Apatite

Årebäck, H., 1995: The Hakefjorden Complex: geology and petrogenesis of a late Sveconorwegian norite-anorthosite intrusion, south-west Sweden. Thesis for Licentiate degree. *Earth sciences centre, Göteborg University A9*.

Aignertorres, M., Blundy, J., Ulmer, P. & Pettke, T., 2007: Laser Ablation ICPMS study of trace element partitioning between plagioclase and basaltic melts: an experimental approach. *Contributions to Mineralogy and Petrology 153*, 647–667.

Green, T., Blundy, J., Adam, J. & Yaxley, G., 2000: SIMS determination of trace element partition coefficients between garnet, clinopyroxene and hydrous basaltic liquids at 2–7.5 Gpa and 1080-1200C. *Lithos 53*, 165–187.

Hart, S.R. & Dunn, T., 1993: Experimental cpx/melt partitioning of 24 trace elements. *Contributions to Mineralogy and Petrology 113*, 1–8.

Hauri, E.H., Wagner, T.P. & Grove, T.L., 1994: Experimental and natural partitioning of Th, U, Pb and other trace elements between garnet, clinopyroxene and basaltic melts. *Chemical Geology 117*, 149–166.

Hofmann, A.W., 1988: Chemical differentiation of the Earth: the relationship between mantle, continental crust, and oceanic crust. *Earth and Planetary Science Letters 90*, 297–314.

Klemme, S., Gunther, D., Hametner, K., Prowatke, S. & Zack, T., 2006: The partitioning of trace elements between ilmenite, ulvospinel, armalcolite and silicate melts with implications for the early differentiation of the moon. *Chemical Geology 234*, 251–263.

Lemarchand, F., Benoit, V. & Calais, G., 1987: Trace element distribution coefficients in alkaline series. *Geochimica et Cosmochimica Acta 51*, 1071–1081.

McCallum, I.S. & Charette, M.P., 1978: Zr and Nb partition coefficients: implications for the genesis of mare basalts, kreep, and sea floor basalts. *Geochimica et Cosmochimica Acta 42*, 859–869.

McKenzie, D. & O'Nions, R.K., 1991: Partial melt distributions from inversion of rare Earth element concentrations. *Journal of Petrology 32*, 1021–1091.

Palme, H. & O'Neill, H. St. C., 2003: Cosmochemical estimates of mantle composition. *Treatise on geochemistry 2*, 1–38.

Paster, T.P., Schauwecker, D.S. & Haskin, L.A., 1974: The behavior of some trace elements during solidification of the Skaergaard layered series. Geochimica et Cosmochimica Acta 38, 1549–1577.

Rudnick, RL. & Gao, Sx., 2003: Composition of the continental crust. *Treatise on geochemistry 3*, 1–64.

Zack, T. & Brumm, R., 1998: Ilmenite/liquid partition coefficients of 26 trace elements determined through ilmenite/clinopyroxene partitioning in garnet pyroxene. *In*: Gurney, J.J., Gurney, J.L., Pascoe, M.D. & Richardson, S.H. (Eds): *7th International Kimberlite Conference*, 986–988. Red Roof Design, Cape Town.

Tidigare skrifter i serien ”Examensarbeten i Geologi vid Lunds universitet”:

404. Preis Bergdahl, Daniel, 2014: Geoenergi för växthusjordbruk – Möjlig anläggning av värme och kyla i Västskåne. (15 hp)
405. Jakobsson, Mikael, 2014: Geophysical characterization and petrographic analysis of cap and reservoir rocks within the Lund Sandstone in Kyrkheddinge. (15 hp)
406. Björnfors, Oliver, 2014: A comparison of size fractions in faunal assemblages of deep-water benthic foraminifera—A case study from the coast of SW-Africa.. (15 hp)
407. Rådman, Johan, 2014: U-Pb baddeleyite geochronology and geochemistry of the White Mfolozi Dyke Swarm: unravelling the complexities of 2.70-2.66 Ga dyke swarms on the eastern Kaapvaal Craton, South Africa. (45 hp)
408. Andersson, Monica, 2014: Drumliner vid moderna glaciärer — hur vanliga är de? (15 hp)
409. Olsenius, Björn, 2014: Vinderosion, sanddrift och markanvändning på Kristianstadsslätten. (15 hp)
410. Bokhari Friberg, Yasmin, 2014: Oxygen isotopes in corals and their use as proxies for El Niño. (15 hp)
411. Fullerton, Wayne, 2014: REE mineralisation and metasomatic alteration in the Olserum metasediments. (45 hp)
412. Mekhaldi, Florian, 2014: The cosmic-ray events around AD 775 and AD 993 - Assessing their causes and possible effects on climate. (45 hp)
413. Timms Eliasson, Isabelle, 2014: Is it possible to reconstruct local presence of pine on bogs during the Holocene based on pollen data? A study based on surface and stratigraphical samples from three bogs in southern Sweden. (45 hp)
414. Hjulström, Joakim, 2014: Bortforsling av kaxblandat vatten från borrningar via dagvattenledningar: Riskanalys, karaktärisering av kaxvatten och reningsmetoder. (45 hp)
415. Fredrich, Birgit, 2014: Metadolerites as quantitative P-T markers for Sveconorwegian metamorphism, SW Sweden. (45 hp)
416. Alebouyeh Semami, Farnaz, 2014: U-Pb geochronology of the Tsineng dyke swarm and paleomagnetism of the Hartley Basalt, South Africa – evidence for two separate magmatic events at 1.93-1.92 and 1.88-1.84 Ga in the Kalahari craton. (45 hp)
417. Reiche, Sophie, 2014: Ascertaining the lithological boundaries of the Yoldia Sea of the Baltic Sea – a geochemical approach. (45 hp)
418. Mroczek, Robert, 2014: Microscopic shock-metamorphic features in crystalline bedrock: A comparison between shocked and unshocked granite from the Siljan impact structure. (15 hp)
419. Balija, Fisnik, 2014: Radon ett samhällsproblem - En litteraturstudie om geologiskt sammanhang, hälsoeffekter och möjliga lösningar. (15 hp)
420. Andersson, Sandra, 2014: Undersökning av kalciumkarbonatförekomsten i infiltrationsområdet i Sydvattens vattenverk, Vombverket. (15 hp)
421. Martin, Ellinor, 2014: Chrome spinel grains from the Komstad Limestone Formation, Killeröd, southern Sweden: A high-resolution study of an increased meteorite flux in the Middle Ordovician. (45 hp)
422. Gabrielsson, Johan, 2014: A study over Mg/Ca in benthic foraminifera sampled across a large salinity gradient. (45 hp)
423. Ingvaldson, Ola, 2015: Ansvarsutredningar av tre potentiellt förorenade fastigheter i Helsingborgs stad. (15 hp)
424. Robygd, Joakim, 2015: Geochemical and palaeomagnetic characteristics of a Swedish Holocene sediment sequence from Lake Storsjön, Jämtland. (45 hp)
425. Larsson, Måns, 2015: Geofysiska undersökningsmetoder för geoenergisystem. (15 hp)
426. Hertzman, Hanna, 2015: Pharmaceuticals in groundwater - a literature review. (15 hp)
427. Thulin Olander, Henric, 2015: A contribution to the knowledge of Fårö's hydrogeology. (45 hp)
428. Peterffy, Olof, 2015: Sedimentology and carbon isotope stratigraphy of Lower–Middle Ordovician successions of Slemmestad (Oslo-Asker, Norway) and Brunflo (Jämtland, Sweden). (45 hp)
429. Sjunnesson, Alexandra, 2015: Spårämnesförsök med nitrat för bedömning av spridning och uppehållstid vid återinfiltrationav grundvatten. (15 hp)
430. Henao, Victor, 2015: A palaeoenvironmental study of a peat sequence from Iles

Kerguelen (49° S, Indian Ocean) for the Last Deglaciation based on pollen analysis. (45 hp)

431. Landgren, Susanne, 2015: Using calcein-filled osmotic pumps to study the calcification response of benthic foraminifera to induced hypoxia under *in situ* conditions: An experimental approach. (45 hp)
432. von Knorring, Robert, 2015: Undersökning av karstvittring inom Kristianstadsslättens NV randområde och bedömning av dess betydelse för grundvattnets sårbarhet. (30 hp)
433. Rezvani, Azadeh, 2015: Spectral Time Domain Induced Polarization - Factors Affecting Spectral Data Information Content and Applicability to Geological Characterization. (45 hp)
434. Vasilica, Alexander, 2015: Geofysisk karaktärisering av de ordoviciska kalkstensenheterna på södra Gotland. (15 hp)
435. Olsson, Sofia, 2015: Naturlig nedbrytning av klorerade lösningsmedel: en modellering i Biochlor baserat på en fallstudie. (15 hp)
436. Huitema, Moa, 2015: Inventering av föroreningar vid en brandövningsplats i Linköpings kommun. (15 hp)
437. Nordlander, Lina, 2015: Borrningsteknikens påverkan vid provtagning inför dimensionering av formationsfilter. (15 hp)
438. Fennvik, Erik, 2015: Resistivitet och IP-mätningar vid Äspö Hard Rock Laboratory. (15 hp)
439. Pettersson, Johan, 2015: Paleoekologisk undersökning av Triberga mosse, sydöstra Öland. (15 hp)
440. Larsson, Alfred, 2015: Mantelplymer - realitet eller *ad hoc*? (15 hp)
441. Holm, Julia, 2015: Markskador inom skogsbruket - jordartens betydelse (15 hp)
442. Åkesson, Sofia, 2015: The application of resistivity and IP-measurements as investigation tools at contaminated sites - A case study from Kv Renen 13, Varberg, SW Sweden. (45 hp)
443. Lönsjö, Emma, 2015: Utbredningen av PFOS i Sverige och världen med fokus på grundvattnet – en litteraturstudie. (15 hp)
444. Asani, Besnik, 2015: A geophysical study of a drumlin in the Åsnen area, Småland, south Sweden. (15 hp)
445. Ohlin, Jeanette, 2015: Riskanalys över pesticidförekomst i enskilda brunnar i Sjöbo kommun. (15 hp)
446. Stevic, Marijana, 2015: Identification and environmental interpretation of microtextures on quartz grains from aeolian sediments - Brattforsheden and Vittskövle, Sweden. (15 hp)
447. Johansson, Ida, 2015: Is there an influence of solar activity on the North Atlantic Oscillation? A literature study of the forcing factors behind the North Atlantic Oscillation. (15 hp)
448. Halling, Jenny, 2015: Inventering av sprickmineraliseringar i en del av Sorgenfrei-Tornquistzonen, Dalby stenbrott, Skåne. (15 hp)
449. Nordas, Johan, 2015: A palynological study across the Ordovician Kinnekulle. (15 hp)
450. Åhlén, Alexandra, 2015: Carbonatites at the Alnö complex, Sweden and along the East African Rift: a literature review. (15 hp)
451. Andersson, Klara, 2015: Undersökning av slugtestsmetodik. (15 hp)
452. Ivarsson, Filip, 2015: Hur bildades Bushveldkomplexet? (15 hp)
453. Glommé, Alexandra, 2015: $^{87}Sr/^{86}Sr$ in plagioclase, evidence for a crustal origin of the Hakefjorden Complex, SW Sweden. (45 hp)
454. Kullberg, Sara, 2015: Using Fe-Ti oxides and trace element analysis to determine crystallization sequence of an anorthosite-norite intrusion, Älgön SW Sweden. (45 hp)

LUNDS UNIVERSITET

Geologiska institutionen
Lunds universitet
Sölvegatan 12, 223 62 Lund